Estimation of Evapotranspiration through remote sensing. Comparison between three different resolution sensors at Barrax field, Spain.

Master's thesis by

John Diego Sierra Torres

Department of Water Resources Engineering

Lund University

Sweden

Abstract
Nowadays importance of water balance regarding measurements and water cycle pathways are of prime interest in a new perspective. Global issues, like Earth warming, or regional planned uses of water, e.g. irrigation, demand an increase in accuracy and coverage of different components of the water balance. Precipitation and the water loss from vegetation and soil, called Evapotranspiration (ET), are main components in the water balance equation. While precipitation, the main input in water balance models, is easily measured, ET, the major loss, is not. Current and most used methods are accurate but limited in time and mostly in space. Extended ET measurements are needed to manage water resources at regional or broader scales with reasonable accuracy. The use of remote sensing has been tested for last two decades and is still subject to extended research to overcome definitively this problem. Present work compares results of application of a simplified version of residual of energy budget, Roerink´s S-SEBI model, to calculate ET using three sensors with high (AHS), medium (ASTER) and low resolution (NOAA´s AVHRR) at Barrax field, Spain, on 18th July 2004. Its application basically stands for energy balance equation using visible and near infra-red radiation measurements coming in and out of the surface-vegetation-atmosphere system. Incoming short and long wave radiation were measured on field at "Las Tiesas" lysimetric station, which was used as reference, and the remaining variables were measured instantaneously at sensors overpasses and then extrapolated to daily values. Jackson empirical model is also used to contrast results. Albedo, temperature and emissivity were retrieved from sensors and used to calculate Evaporative Fraction, net radiation, geothermal flux and vegetation indices NDVI and MSAVI. Once all variables are calculated the S-SEBI is applied and the instantaneous ET value is extrapolated to daily value in mm/day at the chosen area. Results showed a good correlation, for most of variables, between AHS and ASTER and acceptable error (around 10%) for the higher resolution sensor. Meanwhile AVHRR did not show good results but, anyhow, it could still represent some potential use in large and homogeneous areas with less accuracy demand assessments or as complementary information for water resource management at regional or even global scales.

Table of contents

1 Introduction

Almost a third of the Earth dwellers live in vulnerable regions facing water shortage (Millennium Ecosystem Assessment, 2005). These regions, in any case and by the other hand, also deal with population growth and consequently resources demand increase. Water is a limitation in development and optimal use is particularly needed for these demands. In case of irrigation, the highest water demand of all, optimization means the assessment of how much water must be supplied all along the phenological stages of crops. Above this amount it can be consider a waste of resources since water supplied further than this threshold does not imply higher productivity (Wittwer, 1975). ET, as a combined measure of water loss from soil and plants, has had difficulties to be exactly calculated. Except measurements done *in situ* (lysimetric) and covering very limited areas (Oke, 1987), accuracy is hard to attain for extended areas and modelling and indirect methods have to be applied on this purpose, like those using data surveyed by remote sensing techniques (Rodell, 2002). In water and natural resources management large areas have to be evaluated and diverse and complementary information must be gathered in order to get acceptable ET accuracy.

All approaches consider ET as an important fraction of water and energy balances, and although these two balances are, perhaps, the most basic and common balances used in Earth science applications and studies, they also represent a continuous challenge regarding accuracy of their components. If evaporation is measured from a free surface (e.g. water body), its quantification may be regarded easy but, when dealing with ET, water losses through soil and plants involve different phenomena not easy determined; this water transfer includes exchange mechanisms between soil, atmosphere and plants involving biological, mechanical, and meteorological processes comprising many variables. First methods to calculate ET, like Thornwaite`s, used basic climate variables (temperature, and solar incidence-latitude-) neglecting soil, plant and atmosphere interactions taking part (Morton, 1983). Other ground based methods started to include more variables in order to increase accuracy and extension of results (i.e., spatial and temporal) nevertheless and even for small scale estimations, saturation degree of water soil content is hard to measure (especially for extended areas) and thus calculation of real water losses outside the plant-soil system. This problem was partially solved by Bouchet in 1963 with his “Complementary Relationship hypothesis” relating potential (ETp) and actual evapotranspiration (ETa). This was an important contribution towards reliability in estimating ET but still the scale problem was not solved. It was not until mid eighties (Davies and Tarpley, 1983, Price 1982, Jackson 1987) when information from remote sensing complemented ground based methods to extend results to regional and global scales with acceptable accuracy. Since then, many approaches have been made and nowadays continuous optimizations of remote sensing techniques tend towards applicability and accuracy of extended ET estimation. Anyway, remote sensing techniques to retrieve accurate ET values are not considered, at the present, a definitive method itself but a necessary information to complement ground based measurements and then to more extended (in space and time) measurements.

There are many current methods to estimate ET (Jensen et al., 2001). The standard one suggested by FAO is 56 method (Allen et al,1998) which determine ET from reference ET (Penman -Monteith method) from a grazing land under optimal soil moisture conditions using water stress and crop coefficients. Its main difficulty arises from weather and crop coefficients variations for each site. Many remote sensing ET calculations are based on combination of empirical and physical modules (Courault et al ,2005). Among these common methods are those which use residual of energy budget, most used are: SEBAL (Surface Energy Balance Algorithm for Land, Bastiaansen et at., 1998, Jacob et al 2002), SEBS (Surface Energy Balance System, Jia et al, 2003; Su,2002), TSEB (Two source Energy Balance, French et al 2003., Kustas & Norman, 1999) and the S-SEBI (Simplified Surface Energy Balance Index, Roerink et al, 2000) applied in present work to evaluate use of three different sensor resolutions, satellital (NOAAs AVHRR and TERRAs Aster) and airborne (AHS) in computing ET from Barrax field campaign during 18th July, 2004.

1.1 Problem statement

Among all water uses, irrigation represents by far the highest with around 60% of total consumption (WRI, World Resources, 2003- 2004) and if we consider that only 45% out of this water is effectively used by crops (FAO, 2003) then, we would have around 30% of total water consumption lost during irrigation practices. Large basins and regional water managing demand wide-ranging assessments of water availability.

Water balance in dry regions requires high accuracy regarding availability. Water offer determines priority of its uses and is very related to crop productivity (Wittwer,1975) in agricultural uses. The present work area has an aridity index between 15-20, which corresponds to a Mediterranean (semiarid) zone - according to De Martonne- with high losses as evapotranspiration. Despite water scarcity, this zone is regarded as a productive land and water needs for irrigation are of main interest. To have optimal water management and crop productivity, irrigation needs must be assessed accurately. To achieve this, planners need extended measurements of ET but conventional ground based methods (Bowen ratio, eddy correlation system, soil water balance, lysimetric stations, etc) only assess areas limited to available field data that could only be extrapolated to close surrounding areas. For larger scales (i.e. regional, global), differences in land use and local climate variations make difficult to estimate ET with conventional ground based methods, resulting in low accuracy or simply lack of data to correlate (extrapolate), in time and space, values from one place to another. Different methods have been proposed to use remote sensed data in ET calculations (temperature sounders, Heat Capacity Mapping Mission – HCMM, Price 1982 -, energy fluxes balance, etc) but they still have limitations and performance is related to technical features like sensor type number of bands, frequencies, resolution, etc and field conditions like meteorology (most of methods perform better with cloud free images) or surface roughness. Reliable tools to extend temporal and spatial ET data must be improved or developed in order to optimize water uses and follow climate alterations in detail.

1.2 Objective and limitations

The main aim of this work is to compare performance of one airborne and two satellite sensors to retrieve Evapotranspiration (ET) at Barrax field, Spain, on July 18th 2004. The S-SEBI model is applied on this purpose using low resolution NOAA´s AVHRR, and multi-spectral AHS and ASTER. All parameters involved in the ET retrieval are also compared. Besides limitations of the model itself, free cloud images and occurrence of both water saturated and dry areas in the image, conditions that were met by the day of overpass, the major hinder of present work is that just one measurement for each sensor was made and therefore no consistent error theory or validation could be applied. Another limitation is that within all the studied area there are only ET calculations at the meteorological station where the lysimeter covers less area than the AHS pixel, the highest spatial resolution sensor used. This fact focuses the work in comparing the sensors performance, not the model accuracy.

2 DESCRIPTION OF THE AREA

2.1 Site

Barrax is placed southwest Albacete province (39º 30' N, 2º 6' W) at 700m mean height above sea level in La Mancha plateau. The site has been used for several years to carry out agricultural research and due to some of its features as flat land surface, uniform crop fields, etc, since 1991 special emphasis has been given to optimization of remote sensing techniques (Moreno et al., 2001). The chosen area is delimited in table 1 and showed in figures 1 and 2:

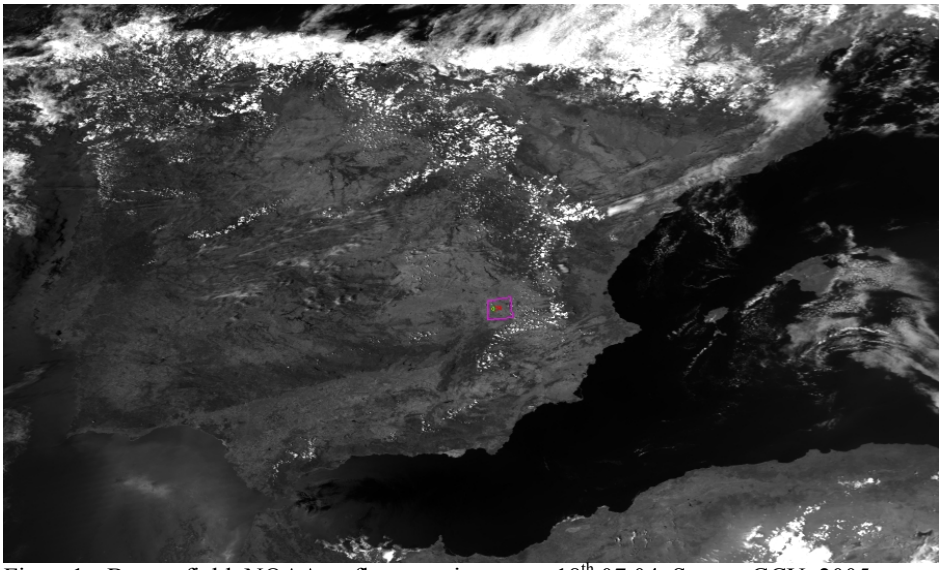

Figure1: Barrax field, NOAA reflectance image on 18th 07 04. Source GCU, 2005

Table 1: *Barrax field corner coordinates*

	Geographical Coordinates	
Corner1	575505.9E	4323210.7N
Corner2	585226.6E	4325555.7N
Corner3	575039.5E	4325144.3N
Corner4	584760.2E	4327489.3N

Figure 2: Test site *S*ource**:** SPARC campaign ,2004

2.2Climatology

The climate of the region is classified as continental with low precipitations. The area has an Aridity index of 17,2 corresponding to a semiarid region (Mediterranean) with precipitation maximum values during spring (April to May) and fall (September to October) and minimum values during summer (July) and winter (January). Highest temperature values are reached in mid summer (July to August) after a gradual increase starting by end of winter (*see graph 1*). Daily oscillations in temperature are significant reaching differences in values around 30º C in summer and 18º C during winter. According to Köppen classification, Barrax area corresponds to Mediterranean tempered climate with hot summers and cold winters.

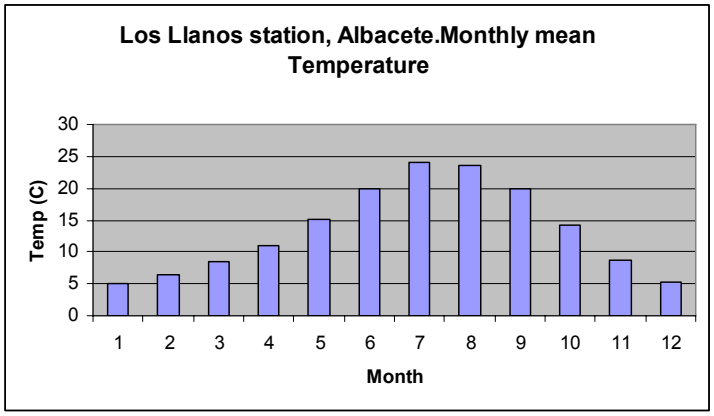

Graph 1: *Monthly temperature Albacete* in ITAP, 2006

2.3 Geology/geomorphology

The area is situated within the La Mancha plateau and has a flat morphology with almost no variations in height (less than 2m). The surface under the Barrax area has several aquifers corresponding to different geological formations. These formations (Holocene, Miocene, Cretaceous and Jurassic) seem to be connected and form a regional groundwater body. The regional water table is about 20-30 m below land surface. Nevertheless, there is some evidence that, at least locally, several perched aquifers exist with their water table between 4 and 7 m deep. (Bolle et al., EFEDA Experiment, 1991)
The soils of the area have been poorly developed. They are very finely textured and have a high degree of compactness under drying conditions featured by calcic sediments with a hard-pan layer. All soils show a calcic hard-pan layer at approximately >40 cm below the surface. The main limitation offered by the soils regarding their productive capacity is the small real depth, due to the presence of the petrocalcic horizon with large amounts of total and/or active limestone. The stoniness is excessive in many cases due to the presence of remains of the petrocalcic horizon on the surface.

2.4 Land use

The prevailing cultivation in the area is approximately 65% dry land (of which 67% are winter cereals and 33% fallow land) and 35% irrigated land with several extensive irrigating

pivots up to 1km of diameter (easily distinguished in the surveyed images). The senescent biomass and vigorous vegetation are distributed in different proportions according to date and crop phenology. (Bolle et al, EFEDA Experiment, 1991)

2.5 Irrigation

According to Ministry of Environment, 83% (higher than global average) of water use in Spain goes to irrigation needs (*White paper on water*, 1998). The total consumption for irrigation in Albacete province, where Barrax is located, is around 402 Hm^3 per year, used systems comprise sprinklers 83%, surface irrigation 16 and 1% local. As said before, Barrax has a 35% of irrigated land, distributed as follows: corn 75%; barley/sunflower 15%; alfalfa 5%; onions 2.9%; vegetables 2.1%.

3 THEORY

3.1 Radiation in remote sensing

Measurement and analysis of the radiant electromagnetic energy coming from target object are the main objective of remote sensing. This energy can be emitted in different ways:

Spontaneous: Originated from the object itself, like γ (gamma) radiation.
Stimulated: Due to the incidence of higher energy level on the object, like infra-red radiation.
Reflected: The object surface is flat or impenetrable by the considered wave length, which is neither altered nor filtrated, just reflected.
Diffused: when the object surface is rough and emits radiation in different directions.

3.1.1 Radiative Transfer

When energy is reflected or diffused, there is always some penetration to the object causing filtration and diffraction. Most of Earth surface behaves this way and when receiving white light rays, emits diffuse and multidirectional light in different colours depending on the object (Kidder and Vonder Haar, 1995). Remote sensing then is based on analysis and measurement of transmitted energy through the electromagnetic spectrum. This spectrum is well extended and just some wide bands, coinciding with atmosphere penetration, are used to get information about the earth (atmospheric windows). Radiations used are: infrared, microwave, and the visible spectrum.

Electromagnetic energy is radiated across space by bodies that posses a temperature above 0 Kelvin (absolute zero). This energy has different properties including the *wavelength* (in μm =10^{-6} m; or nm= 10^{-9}m); the *frequency* cycles per unit time: GHz=10^{9} sec^{-1}) and the intensity. The intensity of radiation (flux per unit area: E=wm^{-2}) is dependent of the temperature of the radiant body, as Stefan Boltzman law indicates:

$$E=\delta T_S^4 \qquad \text{Eq. (3.1)}$$

Where δ (Wm^{-2} K^{-4}) is the Stefan Boltzman constant (5.67 x 10^{-8} W m^{-2} K^{-4})

For most purposes in remote sensing, the sensor is calibrated according to *blackbody* conditions which refer to the efficiency of a body to radiate the maximum amount of energy for a given wavelength or group of wavelengths for a given temperature. A "grey body" in contrast, is less efficient in re-emitting the incident energy relative to its temperature; some of which is attenuated by processes of reflection and transmission . These processes are important in the atmosphere, and the radiation intensity of the earth-atmosphere system is better described by the equation 3.2:

$$E = \boldsymbol{\varepsilon}\, \delta T_S^4 \qquad \text{Eq. (3.2)}$$

where ε is the emissivity.

The emissivity is described by Kirchoff´s law, which can be reduced to the following expression (Eq 3.3):

$$E\ emit / E\ abs = f(\lambda, T) \qquad \text{Eq. (3.3)}$$

where, *E emit* is the intensity of the emitted energy , *E abs* is the intensity of the absorbed energy and λ is the wavelength. Thus, by definition a black body has an emissivity of 1.0 and a grey body $0 < \varepsilon < 1$.The sun approaches blackbody status over most visible wavelengths; however targets in the Earth – atmosphere system may approximate blackbodies only in longer wavelengths. For example snow cover dominates the emission and absorption of thermal infrared radiation (TIR) since it approximates a blackbody in these wavelengths (Foster *et al.,* 1987). Kirchoffs law is valid for materials in *thermodynamic equilibrium* (with the same thermodynamic temperature) and even if this is not always true for some particles present in the atmosphere above 100 km high, for remote sensing purposes the thermodynamic equilibrium is assumed (Vonder Haar, 1995). The spectral distribution of the radiation according to wavelength for a blackbody radiator is given by Plank´s law, which relates the emitted radiation intensity to the temperature, T, and spectral emissivity (Eq 3.4) of the surface:

$$E_\lambda^* = \frac{c_1}{\lambda^5} \frac{1}{e^{\frac{c_2}{\lambda T}} - 1} \qquad \text{Eq.(3.4)}$$

where E* is the total spectral radiation in W/m² , c1 and c2 are first and second radiation constants (3.7413×10^8 W, (μm) ^{4} m^{-2} and $1.4388 * 10^4$ μm K, respectively. The wave length of the maximum emission (λmax), which is inversely related to T, is described by Wien´s displacement law (Eq 3.5):

$$\lambda_m = \frac{2897}{T} \qquad \text{Eq (3.5)}$$

where 2897 is a constant, (μm K).

Cause in nature we can not talk about a perfect absorber/emitter body (blackbody) therefore to see how close materials are from this theoretical state the *emittance* (Eq 3.6) concept of a body is introduced:

$$\varepsilon\lambda \equiv \frac{emitted.radiation.at\lambda}{B\lambda(T)} \qquad \text{Eq (3.6)}$$

where $B\lambda(T)$ is the radiance emitted by a blackbody.

It is function of temperature, viewing geometry as well as wavelength. As said before, emittance for a perfect body equals the unit. Three related quantities describe the fate of radiation incident on a body:

$$\alpha\lambda \equiv \frac{absorbed.radiation.at\lambda}{incident.radiation.at\lambda} \qquad \text{Eq. (3.7)}$$

where αλ is the absorbance at λ

$$\rho\lambda \equiv \frac{reflecteded.radiation.at\lambda}{incident.radiation.at\lambda} \qquad \text{Eq. (3.8)}$$

where ρλ is the reflectance at λ

$$\tau\lambda \equiv \frac{reflecteded.radiation.at\lambda}{incident.radiation.at\lambda} \qquad \text{Eq.(3.9)}$$

where τλ is the tramittance at λ

These three processes are the possible path for incident radiation, by energy conservation each quantity must be less than unit and their sum must be the unit:

$$\alpha\lambda + \rho\lambda + \tau\lambda = 1 \qquad \text{Eq.(3.10)}$$

Different factors affect emissivity of materials (from GCU):

- Nature of emitter body

- Spectral measurement interval (Lyon, 1965; Nerry et al.,1988;Salisbury, 1986)

- Soil water content (Axelson, 1984)

- Emission path (Sobrino and Cuenca, 1999)

Terms emittance and emmisivity appear to be used in a different way. Emittance is the radiant flux leaving a surface per unit area (Barret, 1992) but in some of consulted literature for this work (Kidder and Vonder Haar, *Satellite meteorology*, , 1995, p 56) the

term emittance is referred as the ratio between blackbodies (perfect emitters) and non blackbodies while, in other sources (Carleton, *Satellite Remote sensing in Climatology*, 1991, p 41), this ratio is more common to be defined as emissivity. It describes the efficiency (compared to blackbodies) of the Earth to convert heat energy into outgoing radiation and depends on composition, roughness and water content of surface as well as observation conditions like spatial resolution, viewing angle or wavelength (Jimenez, 2005). Since sensors are calibrated according to blackbody conditions (Carleton, 1991) and the term emmisivity is mostly used in remote sensing literature, latter mentions will be referred to this case.

3.1.2 Radiative Transfer Equation

Quantification and distribution of electromagnetic radiation is the main target in remote sensing techniques. At least within Earth science remote sense applications, Sun is almost the exclusive energy source of this radiation, *i.e.* detected radiation from the Earth (usually called radiance) is the same energy down-dwelling from the sun (usually called irradiance) after interacting with the *Earth-Atmosphere* system. Description of this interacting comprise different pathways, exchanges and alteration of this radiation (see eq. 3.7 to 3.10). Most of retrieval algorithms and estimation techniques have to consider these effects, therefore a general theoretical framework involving the transmission of radiant energy through the atmosphere and all its possible alterations is required. Even if the radiative transfer theory has a background in papers by Lonnel in late 19th century, *Travis et al, 2006,* it was not until the second half of 20th century when the concept of "*energy transfer by radiation in stellar atmospheres*" was introduced by S. Chandrasekhar who applied this theory addressing modern astrophysics concepts. Almost two decades later, behaviour of electromagnetic radiation through the Earth´s atmosphere was described based in those concepts, since then, the solution for the radiative transfer equation was applied to satellite meteorology and remote sensing techniques in different approaches (Travis et al, 2006).

Radiation detected by remote sensors, without considering polarization effects, can be affected by different processes (Kidder, 1995):

-Radiation from the beam can be absorbed by the material (atmosphere). *Term A*.

- Radiation can be emitted by the material. *Term B*

- Radiation can be scattered out of the beam into other directions. *Term C*

-Radiation from other directions can be scattered into the beam. *Term D*

Rate of change of radiation with distance is expressed in Eq 3.11:

$$\frac{dL\lambda}{ds} = A + B + C + D \qquad \text{Eq (3.11)}$$

Where terms A and C are called *depletion terms* since they take away radiation from the beam while *source terms,* B and D, add radiation to the beam. Radiation decrease, integrated over a finite depth of absorber *a* to *b*, is proportional to intensity of radiation and expressed by Beer´s law:

$$L_\lambda = L_0 \exp\left(-\int_a^b \sigma_a(\lambda) ds\right) \qquad \text{Eq.(3.12)}$$

where

$-\sigma a(\lambda) L\lambda$ is term A in Eq 3.11

$\sigma a\ (\lambda)$ in m^{-1}, is *the volume absorption coefficient ($\sigma\beta a(\lambda)$ where ρ (kgm^{-3}) is the density of the absorber and $\beta a(\lambda)$* in m^2K^{-1} is the mass absorption coefficient.

s is the distance

L_0 is the radiance incident on the absorber

And if not scattering assumed, the tramittance (eq 3.9) would be:

$$\tau_\lambda(a,b) = L \exp\left(-\int_a^b \sigma_a(\lambda) ds\right) \qquad \text{Eq.(3.13)}$$

then absorbance (eq 3.7) would be : $1-\tau_\lambda$ and

the emission (Planckian) consider the material (blackbody) as good an emitter as an absorber, term B becomes $+\sigma a(\lambda) B_\lambda(T)$.

If Term C applies (out scattering), it follows Beer´s law and Term C becomes:

$-\sigma s(\lambda) L_\lambda$ where, $-\sigma s\ \lambda$ is the volume scattering coefficient.

Finally term D, considering all directions scattered into the beam, is expressed :

$$Term\ D = +\frac{\sigma_s(\lambda)}{4\pi} \int_0^{2\pi} \int_0^{\pi} L_\lambda(\theta`,\phi`) p(\psi_s) \sin\theta` d\theta d\phi, D \qquad \text{Eq.(3.14)}$$

where $(\theta`,\phi`)$ is the direction of incoming radiation and ψ_s is the scattering angle (between $\theta`,\phi`$ and θ,ϕ):

$$\cos\psi_s = \cos\theta\cos\theta` + \sin\theta\sin\theta`\cos(\phi - \phi`) \qquad \text{Eq.(3.15)}$$

where $p(\psi_s)$ is the scattering phase function, which for an isotropic scatterer equals 1. In this case term D becomes:

$$\text{term } D = \sigma s(\lambda)[\ L\lambda`] \qquad \text{Eq. (3.16)}$$

where $[L\lambda`] = \frac{1}{4\pi}\int_0^{2\pi}\int_0^{\pi} L_\lambda(\theta`,\phi`)p(\psi_s)\sin\theta` d\theta` d\phi`$ Eq.(3.17)

finally adding all terms, the *radiative transfer equation* for nonpolarized radiation is:

$$\frac{dL_\lambda}{ds} = -\sigma_a(\lambda)L_\lambda(\theta,\phi) - \sigma s(\lambda) L_\lambda(\theta,\phi) + \sigma a(\lambda) B_\lambda(T) + \frac{\sigma(\lambda)}{4\pi}\int_0^{2\pi}\int_0^{\pi} L_\lambda(\theta`,\phi`)p(\psi_s)\sin\theta` d\theta` d\phi` \quad \text{Eq.(3.18)}$$

Substituting eq. 3.18 and rearranging, it becomes:

$$\frac{dL_\lambda}{ds} = \sigma_a(\lambda)\left[B_\lambda(T) - L_\lambda(\theta,\phi)p\right] + \sigma_s(\lambda)\left[\left[L_\lambda`\right] - L_\lambda(\theta,\phi)\right] \quad \text{Eq. (3.19)}$$

The *first* term on the right accounts for absorption and emission, if $\sigma_a(\lambda)$ is zero, the layer (atmosphere) is transparent absorptionally, *i.e.* the beam passes through it unchanged. If $\sigma_a(\lambda)$ is not zero, temperature of the layer and the radiance itself determine the change in the beam. The beam increases if $B_\lambda(T)$ is greater than $L_\lambda(\theta,\phi)$ and decreases if opposite. *Second* term on the right accounts for scattering. If no scattering particles are present $\sigma_s(\lambda)$ is zero; if present, the beam increases if the directionally weighted average radiance $\left[L_\lambda`\right]$ is greater than the beam radiance $L_\lambda(\theta,\phi)$ and opposite (the beam decreases if $\left[L_\lambda`\right] < L_\lambda(\theta,\phi)$).

Because some degree of complexity and mainly due to simplifications are used in remote sensing (Kidder et at, 1995), the extended formal solution is not showed nor used in present work. As a reference, Goody and Yung present the formal solution in a work (1989) if any reader interested.

The first two terms on the right side of eq. (3.19) can be combined to form $-\sigma_e(\lambda)$ $L_\lambda(\theta,\phi)$, where:

$$\sigma_e(\lambda) \equiv \sigma_a(\lambda) + \sigma_s(\lambda) \quad \text{Eq. (3.20)}$$

is called the *volume extinction coefficient.*

If the equation is divided by this coefficient and a new variable is introduced, δ_{sl}, the *slant path optical depth*:

$$\delta_{sl}\left(s_1, s_2\right) \equiv \int_{s1}^{s2} \sigma_e(\lambda, s) ds \quad \text{Eq.(3.21)}$$

Since meteorological variables are commonly known as a function of height, z, rather than slant path, s, n the *vertical optical depth* is introduced:

$$\delta\lambda(z_1, z_2) \equiv \int_{z1}^{z2} \sigma_e(\lambda, z)dz \qquad \text{Eq.(3.22)}$$

Since the Earth radius is much thicker compared with the Earth atmosphere, both optical depths can be related:

$$\delta_{sl}(s_1, s_2) = \frac{\delta(z_1, z_2)}{\mu} \qquad \text{Eq (3.23)}$$

where μ is the cosine of the zenith angle θ, z_1 correspond to s_1,and z_2 is s_2. The *vertical optical depth,* δλ, between the surface and level z can be expressed as, δλ= δλ (0,z), thus, $d\delta_\lambda = \sigma dz = \mu\sigma_e ds$. Other two concepts are introduced:

$$\alpha_\lambda \equiv \frac{\sigma_a(\lambda)}{\sigma_e(\lambda)} \qquad \text{Eq (3.24)}$$

called the *absorption number* and

$$\omega_\lambda \equiv \frac{\sigma_s(\lambda)}{\sigma_e(\lambda)} \qquad \text{Eq (3.25)}$$

the single scatter albedo.

Including these two concepts, the radiative transfer equation becomes:

$$\mu\frac{dL_\lambda}{d\delta_\lambda} = -L_\lambda(\theta,\phi) + \alpha_\lambda B_\lambda(T) + \frac{\omega_\lambda}{4\pi}\int_0^{2\pi}\int_{-1}^{1} L_\lambda(\mu`,\phi`)p(\psi_s)d\mu`d\phi` \qquad \text{Eq (3.26)}$$

cos θ substitutes μ.

Two common general simplifications assume non scattering and non emission conditions:

For practical purposes two common general simplifications assume non scattering and non emission conditions:

One is known as Schwartzchild equation which neglects scattering and is commonly used for non cloudy condition in the infrared region (Kidder, 1995), its general formulation, using the same notation proposed above, is:

$$\mu\frac{dL_\lambda}{d\delta_\lambda} = -L_\lambda(\theta,\phi) + B_\lambda(T) \qquad \text{Eq (3.27)}$$

Other common simplification represents a *non emission equation* since the Earth-atmosphere system emits no significant radiation at visible or near infrared wavelengths:

$$\mu \frac{dL_\lambda}{d\delta_\lambda} = -L_\lambda(\mu,\phi) + \frac{\omega_\lambda}{4\pi}\int_0^{2\pi}\int_{-1}^{1} L_\lambda(\mu`,\phi`)p(\psi_s)d\mu`d\phi` \qquad \text{Eq.(3.28)}$$

If we compare this equation with eq.(3.26) it is seen that it is almost identical but the in this case the Plank emission, $B_\lambda(T)$, is neglected.

It was already mentioned that use of radiative transfer equation is common in deriving remote sensing techniques. Since methods and retrieval algorithms are normally based on semi empirical and /or statistical relationships (see chapter 4 pages 34 to 40) solutions can be found assuming simplifications according with field conditions and validation capacity. For instance, retrieval algorithms neglecting scattering effects are used in cloud free images since infrared radiation is not considerably affected in these cases (Kidder, 1995). Another simplification assumes that at visible wavelengths absorption by liquid water or vapour (clouds) is negligible (Kidder, 1995).

3.2 Radiation commonly used in remote sensing

3.2.1 Solar radiation

Electromagnetic fields oscillate rapidly and transfer energy as radiation, photons and waves associated to photons. Photons transport bundles of energy known as quantum. It is expressed so:

$$Q=h*v=h\ C/\lambda \qquad \text{Eq (3.29)}$$

Where h is The Plank constant ($6.625x10^{-4}$), λ is the wavelength, v the frequency and C the velocity of wave propagation (≈300.000 km /s), then:

$$v= C/\lambda \qquad \text{Eq.(3.30)}$$

λ can be expressed in meters (m), micron (μ) or Ångstrom (Å). Frequency is expressed in hertz.

3.2.2 Electromagnetic Spectrum

Solar radiation is a complex mixture of radiations with a spectral distribution (energetic flux) in function to its wavelength:

$$\Phi=\int_{\lambda_1}^{\lambda_2} \phi_\lambda(\lambda)\, d\lambda \qquad \text{Eq(3.31)}$$

where
Φ=emitted flux in a spectral band between λ1 and λ2
λ1 and λ2 = wavelength limits in between the received flux.
Φλ= energetic flux of the spectrum

Solar spectrum (fig 3) reaching the earth has a maximum illumination at 0,5 μm. Near 45% of the incoming radiation is received in the visible range (0,4 and 0,7μm). When radiations enter into the atmosphere, its gases absorb some of this radiation in a selective way, thus ozone absorbs wavelengths less than 0,29μm (harmful to life) and reduces some of red ones corresponding to 0,6μm. Oxygen absorbs 0,76μm wavelengths in a very narrow strip. In turn, water vapor and CO2 absorb infrared radiations mostly. Almost all visible radiation gets through the atmosphere and just some bands of spectrum (atmospheric windows), like those of 8 and 14μm in the thermal infrared. Land receives global radiation comprising direct and diffuse radiation, which is very variable depending on day time, weather, latitude or season.

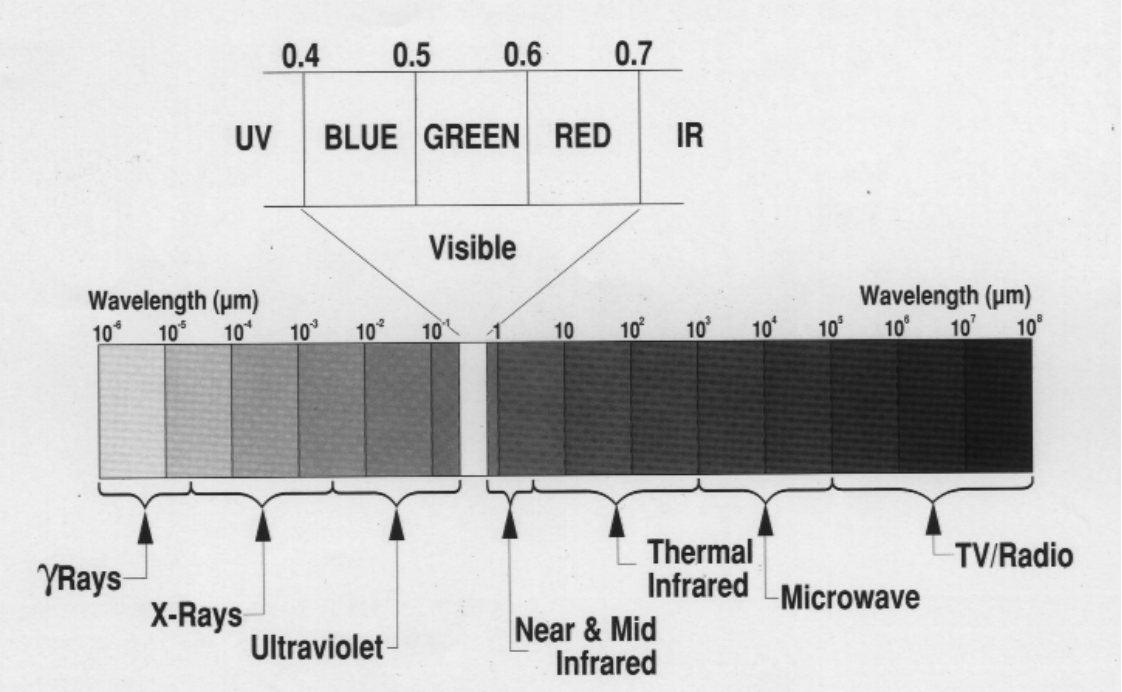

Figure 3. *Bands of Electromagnetic Spectrum (from www.casde.unl.edu)*

If we take average temperatures for the sun, 6000 K and 300K for the Earth, then we have a maximum emission values of 0.5 and 1.0 μm respectively meaning solar radiation reaches its peak at short wavelengths (higher frequencies) of visible light (0.4-0.7 μm) while radiation emitted by the Earth-atmosphere system peaks in lower frequency bands, the TIR (8-14 μm).

Visible radiation - between 0.4 and 0.7μm- is placed in a very narrow range of the electromagnetic spectrum reaching the Earth. Not even radiations less than 0,2 μm (up to 1nm), corresponding to X, λ and ultraviolet rays, play an important role in the Earth – atmosphere system. Main radiation detected in the atmosphere – Earth- surface system include:

-Reflection of shortwave solar radiation (albedo) which is integrated across all the visible wavelengths

- The thermal infrared (TIR) emission of Earth corresponds to physical temperature (T)
- Microwave radiation from the Earth surface useful in meteorology to calculate gases profile and humidity content.

3.2.3 Long and short wave natural radiations

Actually, all the solar radiations are comprised between 0, 15 and 4µm. By the other hand, Earth´s energetic flux is placed among 3 and 100µm. This means solar and earth radiation are overlaid in a little strip among 3 and 4µm, lower than these are short wavelengths and upper are the long wavelengths.

3.2.4 Atmospheric Radiations

Water vapor, CO2, aerosols and ozone emit thermal infrared radiations downwards the Earth surface. These radiations have very long wavelength, 5 to 100µm, and can be calculated in different ways, one is the Brutsaert formula:

$$M_{La} = E_{La} = 1.24(\frac{e_a}{T_a})^{\frac{1}{7}} \sigma T_a^4 \qquad \text{Eq (3.32)}$$

where:

δ = Boltzman constant (5,669 *10 $^{-8}$ W/m²K^4
MLa= atmospheric radiation (exitance)
ELa= Atmospheric illumination, at surface level equals to MLa.
ea= vapor tensión (humidity)
Ta= Temperatura(K)

3.2.5 Earth radiations

Earth radiation depends on the body or the emitting material. Atmosphere absorbs Earth radiation, except in the atmospheric window between 8 and 14µm if atmosphere is clear; if cloudy, they absorb the Earth radiation and get a half back to the earth (greenhouse effect).

3.2.6 Net radiation

It is the balance of all incoming and outgoing radiations in all the Earth wavelengths, according to WMO is expressed in Eq 3.33:

$$E = (Eg\downarrow - Mg\uparrow) + (EL\downarrow - ML\uparrow) \qquad \text{Eq.(3.33)}$$

where:

E= net radiation
Eg ↓ = global radiation
Mg↑=short wavelength exitance
EL= long wavelength illumination (radiation)
ML= long wave exitance

Earth absorbs part of the global and atmospheric radiation, reflects some of both and emits earth radiation. It also can be expressed:

$$Eg\downarrow - Mg\uparrow = Eg\downarrow - \alpha\ Eg\downarrow = (1-\alpha)\ Eg\downarrow \qquad \text{Eq(3.34)}$$

where α =earth albedo.

$$\text{Besides, } H = A\ Hg\downarrow - B \qquad \text{Eq (3.35)}$$

H=net energetic exposure
A, B= empirical parameters
Hg ↓= global energetic exposure.

This climatic parameter is very useful to calculate water needs in agro forest activities. Balance of radiations depends also on other factors like albedo, thermal conductivity, surface emissivity, evapotranspiration, topography, and wind direction.

3.2.7 Surface Albedo (α)

Albedo is a key factor to understand the Earth energy balance and is defined "as the ratio of the amount of shortwave radiation reflected to the total incident. The reciprocal of this quantity (1-α) gives the amount of shortwave energy which, along with the infrared emittance, comprises the surface net radiation. The last is partitioned into the sensible and latent heat fluxes, thus (after Henderson-Sellers and Wilson, 1983)":

$$(1-\alpha_s)\ R_s = \varepsilon\ (\sigma\ T_s^4 - R_L) + SH+LH \qquad \text{Eq (3.36)}$$

where
ε is the infrared surface emissivity
T_s is the surface temperature
R_L is the downward thermal radiation
R_s is the amount and nature of incident solar flux at surface
SH and LH are the sensible and latent heat fluxes.

Albedo is one of the most common parameters retrieved from satellites. Even if its compute is made using a simple operation between visible bands (average and weighting factors in most cases), acquiring reliable data still represents some difficulties. Carleton summarizes the most important four:

(1) *The surface characteristics and their interaction with the shortwave radiation:* Distinctions between land and sea at similar latitudes (e.g., Saunders and Hunt, 1980) for large scale and land use variations for meso-scale observations as well as soil moisture influence. At lower scales influences of surface roughness, soil particle size and texture, leaf size and orientation, and others, are also important when evaluating acquired data.

(2) *The characteristics of the intervening atmosphere*: Besides attenuation due to scattering or absorption by ozone and water vapor in the near IR, which can be modelled, the optical depth (transmissivity) of the atmosphere is highly influenced by aerosols. These vary spatially and temporally. Accordingly, concurrent observations of the atmospheric state are normally required, or assumptions made about the spatial gradient of the optical depth (see, e.g., Pinty and Szejwach, 1985). Other problems arise as the spatial resolution of the sensor degrades and for low clouds over the ocean, as the sun's elevation above the horizon becomes low (Taylor and Stowe, 1984).

The amount of reflected solar energy depends on the sun's elevation and the direction of reflectance (Pinker, 1985).

3.3 Solar radiation and optical properties of the surface

Ground (surface) receives part of the global and atmospheric radiation, part is reflected and it also emits its own radiation. Soil loses heat by infrared radiation proportional to the difference between its temperature and atmosphere apparent temperature. Energy differences between soil and atmosphere and low and high latitudes generate the atmosphere general circulation, which is a key factor to atmosphere-soil energetic balance (Seoanez, 1991).

Reflectance of soil or ratio between reflected oxitance by a flat surface and its illumination increases from visible spectrum to mid infrared. The same happens to vegetation, there are bands corresponding to water absorption increasing as humidity increases. Besides that, soil reflectance decreases as humidity increases. Soil has more reflection capacity in the visible and mid infrared spectrum than vegetation but much less in the near infrared. Soil reflectance depends on water content, roughness, relief, organic matter content, and composition. Minerals have reflectance spectrum partially overlaid (except iron) causing a continuous variations which are high in sulphates and carbonates presence. Organic matter is also an important factor affecting soil optic properties, if higher than 3%, reflectance is reduced in the visible and near infrared. Organic matter content also increases water retention altering its structure and reducing its reflectance. If soil particles are very small, they shape an apparent flat surface, increasing reflectance. Relief and roughness are also important, when increasing, reflectance is reduced, it is even more important than presence of vegetal cover. Orientation, slope and the incoming angle of radiation are other determining factors and reflectance is high when less shadowing is present. Energy intensity changes with incoming angle, for surfaces formed

by rocks, grooves and relief contrasts, *Lambert s law* or perfect diffusion of surfaces (all directions reflection) is not applied.

3.3.1 Solar radiation and optical properties of vegetation

We know part of incident energy is used by photo synthesizers, it is transformed and accumulated to photochemical energy to convert into organic matter (vegetation). Out of all the incoming radiation to vegetation it just capture around 1 to 2,5%. Optical properties of vegetation mass depend on species, place and nature of leaf system and even on the type of supporting soil. Diffusion of light made by leaves is due to:

- Discontinuity of reflection index in hydrated walls of the plant
- Free water between cell spaces.
- Air content in parenchyma tissue.

Reflectance of leaf organs to perpendicular radiations is due to diffusion of light caused by inner tissues, but if incident angle changes from perpendicular, mirror reflection begins to be important. Thus, solar radiation only penetrates leaf tissues partially depending on reflectance of these organs and:

- number of cells
- thickness of parenchyma
- Leaves with thrycomas increase reflectance in the visible spectrum and mid infrared but not in the near infrared.
-

The upper part of the leaves has less reflection capacity than lower part. Reflectance of leaves decreases when increasing water content as well as soil like mentioned before (see *figure 4*). Reflectance also decreases when nitrogen content diminishes. Finally, it can be said that parasites and leaf diseases alter pigments or water content, incident in optical properties (reflectance) of these organs.

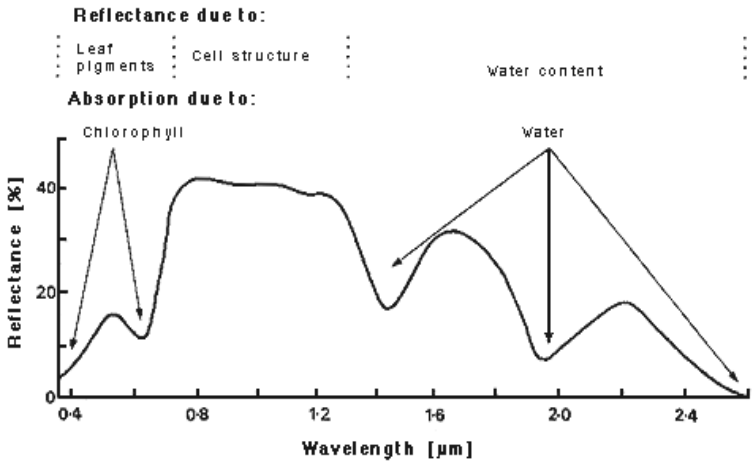

Figure 4. Typical Reflectivity curve for healthy vegetation. (Swain and Davis, 1978)

3.3.2 Luminous energy and vegetation cover

Luminous energy affects growing and developing processes of vegetation and others like transpiration. By the other hand, one important process is transformation of luminous energy into photochemical during photosynthesis at short wavelengths between 0,4 t 0,7µm (PAR), it can be indicated that:

$$Q_c = \int_{\lambda_1}^{\lambda_2} n(\lambda) \frac{hC}{\lambda} \, d\lambda \qquad \text{Eq(.3.37)}$$

where:
Qc= Radiant incident energy between λ λ
λ 1 λ2= Wavelengths
n(λ)= Photons received in wavelength λ
h= 6,625* 10^{-34} J *seg (Plank s constant)
PAR= Photosynthetically Active Radiation.

It is known that PAR is about 50% of the incoming solar radiation and that photosynthesis is reduced and may be 0 in lower leaves of vegetation cover, if this is dense. The respiration-photosynthesis process can be summarized saying that during dark phase, vegetation consumes oxygen and glucids, stored during daytime, and emits CO_2, getting to the end of the night to negative photosynthesis values. At the beginning of the day, this negative value starts to reduce until it reaches an equilibrium point or *compensation point,* then luminous energy received by the plant reaches a net positive value. In a similar way and at the same time CO_2 produced by respiration is equalized by the CO_2 absorbed during photosynthesis, and from this point, it continues increasing until the maximum net assimilation, along whole the day till night. From this moment the process is independent from luminous energy received by the plant. This level of saturation depends on vegetation species and CO_2 concentration, if this concentration increases temperature can influence and increases the process activity.

3.3.3 Vegetation indices

Vegetation indices are helpful parameters in remote sensing to minimize influence of external factors like soil optic properties, irradiance (solar incoming radiation), atmospheric perturbations, etc. Red and near infra red bands are used to compute vegetation indexes since they comprise 90% of information about vegetation cover (GCU). Most used are:

- *RVI (Ratio Vegetation Index, Person and Miller,1972):* More sensible to Earth optical properties than illumination conditions.

$$RVI = \frac{\rho ir}{\rho r} \qquad \text{Eq(3.38)}$$

where ρr and ρir are visible (red) and near infrared radiation respectively.

- *NDVI* (*Normalized Difference Vegetation Index*, Rouse et al 1974): chlorophyll, the green pigment responsible for photosynthesis, reflects most of near infrared radiation and absorbs radiation in the visible (red) (see figure 4).Compared to this, water in different phases has opposite reflectances, higher in the visible than in near infrared, while rocks and bare soil show similar values for the same bands. This contrast is useful to differentiate land features since greener and dense vegetation have high NDVI values (up to 0,6), rocks and bare soil show values close to 0 and snow, rivers and clouds normally have negative values (Richards, 1986). Normalization is applied to remove effect of varying sun angle and viewing angle (Vonder Haar, 1995) and is made by dividing the difference between near infrared and red bands by its addition, as showed in the formula:

$$NDVI = \frac{\rho ir - \rho r}{\rho ir + \rho r} \qquad \text{Eq (3.39)}$$

where ρr is red radiation and ρir the near infrared radiation.

MSAVI (Modified Soil Adjusted Vegetation Index, Qi et al, 1994): This is another vegetation index that takes advantage of contrast between red and infrared radiation reflected from vegetation minimizing effect of bare soil (GCU). It is based on a modification of NDVI called SAVI (Huete,1988) where vegetation spectral response is isolated by removing soil moisture effects. MSAVI is not as sensitive to changes in vegetation as NDVI but is more sensitive to atmospheric changes than the NDVI (ESRI, Technical paper, 1998).

$$MSAVI = \frac{2(\rho ir + 1) - \sqrt{(2\rho ir + 1)^2 - 8(\rho ir - \rho r)}}{2} \qquad \text{Eq (3.40)}$$

where ρr and ρir are red and infrared radiation.

LAI (Leaf Area Index, Choudhury, 1986): this index specifies the ratio between vegetation cover and ground area. It can be computed by statistics using direct sampling in the crop or by indirect methods based on light extinction comparing light levels by crop canopy and ground (FAO,1985).

ARVI (Kaufman and Tanré,1992)
For specific applications in areas with atmospheric contamination, the ARVI (Atmospheric Resistant Vegetation Index) index is introduced. It reduces aerosols impact using reflectivity values in blue region:

$$\text{ARVI} = \frac{\rho ir - 2\rho r + \rho b}{\rho ir + 2\rho r - \rho b} \qquad \text{Eq (3.41)}$$

where ρb is the blue reflectivity.

3.4 Soil and climate

3.4.1 General properties of soil

Energy balance can be expressed:

$$E+\Phi_s+\Phi_h+L\,\Phi_w=\rho c_h\,\frac{dT}{dt} \qquad \text{Eq (3.42)}$$

where

ρ =Specific mass
ch= thermal mass capacity
T= temperature
E=net radiation
Φs= heat flux density by conduction in the soil
water = heat flux density by conduction in the air
L= water vaporization latent heat
Φw= water vapor conductive flux density
ρch dT/dt= heat change stored in vegetation cover or bare soil.

Soil properties may affect 2 terms of this formula, the net radiation (E) and stored heat $\rho c_h\, dT/dt$. Radiation captured by soil is highly variable and can be expressed as follows:

$$E= (1-a)E_g -\varepsilon_s\delta(T_s^4- T_A^4) \qquad \text{Eq (3.43)}$$

where

E= net radiation
a= albedo
Eg= global radiation
εs= soil emissivity
δ=Stefan Boltzman constant
Ts= soil surface temperature
TA= atmosphre radiant aparent temperature

Dark soils, with low albedo, are heated more rapidly, reason why vegetation sprouts and begins before its vegetative period, affecting microclimates.

3.4.2 Soil and albedo influence

Reflection capacity of soil depends mostly on color and water content. When darker, less reflection and more absorption of radiation (as heat) is produced. Albedo is the fraction of solar radiation that its reflected by a surface. Water content in soil affects albedo absorbing radiation and decreasing reflection with a variation between 10 to 20% respect to dry soil. Albedo is influenced by daytime, slope, direction and latitude. Next, reflection capacity and albedo of different materials are shown:

Table 2. Reflection capacity of solar radiation for different soils

Clear soils	*Reflection*	*Dark soils*	*Reflection*
White	85	Black	5
	80	Black sand	10
	55	Dark soil	15
	40	Dark rocks	20
	38	Dark sand	20
Gray	30		

Table 3: Albedo for different surfaces

From Vonder Haar

surface	*Albedo*	
	In μm	*In %*
Water	*0,03-0,5*	*5-70*
Snow	*0,4-0,95*	*60-99*
Ice	*0,2-0,4*	*20-40*
Sand	*0,2-0,45*	*20-30*
Bare soil	*0,1-0,35*	*10-25*
Road	*0,05-0,1*	*5-10*
Prairie	*0,16-0,26*	*25*
Cereal crops	*0,1-0,25*	*10-25*
Deciduous forests	*0,1-0,2*	*5-10*
Conifers	*0,05-0,15*	*5-10*

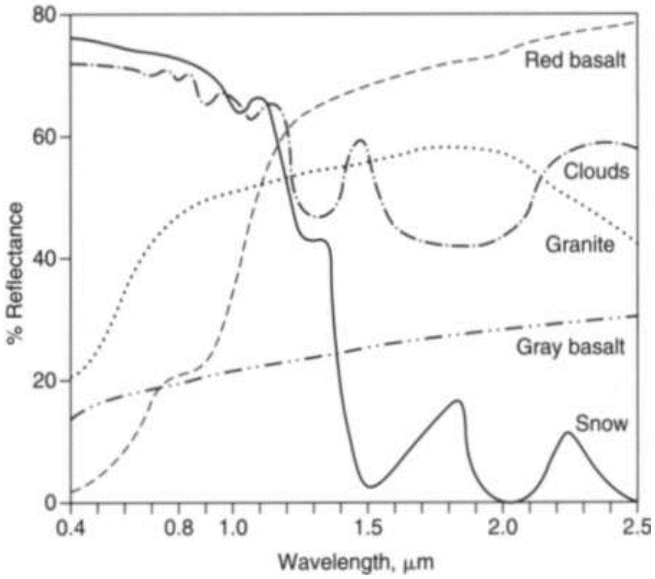

Figure 5 Reflectance for different rocks and clouds
In GCU guide.

3.4.3 Influence of soil thermal conductivity

Soil influences air temperature according to thermal conductivity of both. When thermal conductivity of air is high, solar radiation slowly heats up soil to some depth, reaching maximum temperatures at 5cm depth 2 hours after being maximum at surface and 10 to 15 cm 5 hours later (Kohnke,1994). Soil thermal conductivity depends on:

- *Thermal constituents of forming particles.*
- *Particle size.*
- *Soil porosity.*

- *Soil humidity.*

If the soil is moist, its thermal conductivity increases, cause water is a good thermal conductor and solar radiation, as heat, penetrates deeper into the soil. Clay soils last longer to heat and cold than others, thus, at night they preserve heat acquired during day. Otherwise is the case for sand, which heating and cooling are much faster. Ploughed soils have low conductivity cause of high porosity. Regarding air, its thermal conductivity increases with wind velocity, high temperatures or relative humidity. So, thermal conductivity of air is bigger when turbulences, thermal convection or high water vapor are present. At these conditions, high conductivity is present and heat is transmitted rapidly across the air mass and few changes in temperature occur. If thermal conductivity is low, the thin atmospheric layer in contact with soil is heated or cooled intensely.
Lower cloud masses make the air temperature to have few changes due to interception of solar radiation which is reflected and emitted causing temperature increasing in the air mass.

3.4.4 Humidity and permeability influence

Evaporation causes a heat loss, thus during summer, a moist soil is colder than a dry one. When the weather is calm, there is low evaporation, little heat loss and constant high temperatures. If wind is present water vapor is dispersed increasing evaporation. This process may have even high rates if soil water particles go to the atmosphere and water equilibrium shifts to soil. With impervious soils like clay, evaporation is important after rain, a temperature drop is caused but when water source ceases, temperature increases again. If soil is permeable, contrast is lower cause there will always be water source from soil or air. In marshes and bogs, with permanent moisture, thermal conductivity of soil is very high and oscillations are low. Haze and fog are frequent. In clay surfaces, during rainy days will be temperature fluctuations and haze and fogs presence.

When sky is clear, calm conditions and proper humidity are present, soil becomes determining to temperature and humidity causing horizontal, vertical precipitations and winds.

3.4.5 Solar radiation and soil temperature

Earth surface is heated by solar radiation. It is also important to consider:

- Microbial activity in soil is effective between 0 and 40°C, out of this range activity is almost zero.
- Some chemical reactions are intensified and catalyzed when temperature increases.
- If temperature increases, loses as counter -irradiation and conductivity increases preventing that increasing be too high.
- Bare soils heat more than vegetated areas due to lack of interception of radiation.

- Water regulates soil temperature and transmits downwards, if wet, temperature fluctuations of surface. This is done regulated and steadily, but when soil is dry, temperatures change rapidly as they evolve outside.
- Soil temperatures can be shown in a *thermal profile,* indicating values for different horizons similar to atmosphere thermal profile.
- Drainage contributes with soil heating during spring.
- If surface is covered with snow, extreme temperature can drop substantially, while soil temperature just decreases to –2 to -1°C.
- An organic matter cover regulates soil temperature respect to exterior lowering during summer and regulating it during winter.

3.4.6 Thermal conductivity of soil

Thermal conductivity of soil is the amount of heat flux through $1cm^2$/seg in a vertical thermal gradient of 1°/cm perpendicular to surface with no more heat transmissions, it is expressed in Eq 3.44:

$$Q=\lambda \frac{dT}{dx} \qquad \text{Eq (3.44)}$$

where

Q= transferred heat per area in time or heat flux units
λ =Thermic conductivity
T=temperature
X= soil depth

Temperature of soil depends on transported heat and its specific volumetric heat (absorption capacity). Heat flux indicated in the formula is positive when it is ascending and negative when descending. If increasing with depth, temperature will raise and accumulate heat, if decreasing it will lower and lose heat. Control and movement are described by different curves:

- *Isotherms: in a diagram relating soil depth-time*
- *Isotherms: in a diagram relating temperature-time*
- *Tautochrones (or instantaneous): in a diagram relating temperature-soil depth*

Heat conductivity values (in W/mK) for different soil compounds ranges from 0,15 for dry sand or dry soil with organic matter to 4 for saturated sand or soil while clayish soils range from 0,6 to 2,5 depending also on moisture contents. By the other hand, rocks have much higher values with values up to 7 for solid rocks and values between 0,5 to 2,5 for porous ones (Hukseflux, 2001).

3.4.7 Surface and soil temperature

Some features are summarized:

- Wet soils, with high thermal conductivity, have a proper constant related with dry soil and another one related with water content, according to volume and concentration.
- During winter, soil temperature has less influence on the air temperature.
- During summer, radiation generates high temperatures conditioning temperature near soil.
- Sandy soils are highly heated on surface but not in depth.
- Granitic soils are heated at surface and depth.
- Death vegetation biomass covering soil has a low thermal conductivity.
- Soils with high thermal conductivity melt contacting snow faster.
- More than 10m deep, soil is colder during summer than winter

3.4.8 Vegetation effects on climate

Climate differences presented in a determined area are basically due to:

- Topography: mainly slope and orientation
- Soil type: influencing thermal diffusion.
- Forest areas: when placed on hillside, formation of cold air masses downwards the valley conditioning the area.
- Grassed lands: also change according to climate conditions
- Agricultural areas and Water bodies

Vegetation species diversity is due to climatic variations, but vegetation cover also modifies climatic conditions. This modification is based on:

- Roughness change
- Variation in caloric balance (due to albedo variation)
- Relative humidity and temperature variations.

Roughness variation: the higher the roughness, lesser the wind velocity, higher stress. This is influenced by plant height, size, forest density, age and season. Forests increase roughness by:

- the density of vegetation cover
- thickness of vegetation cover
- If trees in the forest have different height, roughness is increased.

When an air mass, coming from a plateau, gets across a forest, it is slowed down and raised, increasing rain. When air is getting out from the forest, it increases velocity diverging and creating a subsidence.Air flux is turbulent inside the forest. Opposite happens when the vegetation cover is scarce and the flux is laminar.

3.4.9 Territory climate and relation with vegetation

Climate is an important ecological factor influencing geographical distribution of vegetation species. This distribution is known by a principle: "*Distribution of plants is*

first controlled by distribution of climate conditions in a particular place, where extreme conditions can have more significance than average values".
Climate influences species distribution as follows:

1. Acting directly over vegetation species organs.
2. Acting indirectly over processes shaping supporting soil.

To analyze climate variation, average values of climatic variables are used, and that variation determines their distribution. Climatic variation is the evolution of atmospheric conditions during a considerable period. Variability can be thermal, barometric, pluviometric, etc. Climate influence on vegetation show flora and morphology characteristics clearly (Seoanez, 1991).

3.4.10 Caloric balance variation

Heat inlet implies:

- Soil heating by conduction
- Transformation of water into water vapor due to evaporation and evapotranspiration.
- Transformation of received energy to organic matter through photosynthesis
- Air heating

Surface albedo changes, including soil and vegetation, affect energy and radiation balance and depend on percentage and shape of vegetation cover. It is known that albedo does not change much if vegetation cover is dense and homogeneous and sometimes independent of the type of vegetation, for instance, it is around 0,25 for a forest mass or for a beetroot crop. If vegetation cover is not dense and regular, albedo values are variable due to differences in height. Lower vegetation reflects part of the radiation which is intercepted by higher trees, part is reflected to soil and part is reflected to atmosphere. Within a forest temperature stays attenuated due to:

- -Heat storage
- -Interception of this heat by vegetation cover moderates temperatures (making higher minimums and colder maximums).
- The floor of a forest is slightly hotter by night and about 4 to 5ºC colder during day, compared with canopy.
- Net radiation received by forests is bigger than received by prairies due to difference between absorption coefficients (less for prairies).
- Green color predominant in forests is related re-emission of red and yellow wavelengths.
- Incoming radiation to inner forest is low in ultraviolet and high in infrared radiations.

3.4.11 Relative humidity variation

Plant transpiration releases water into air. In areas with important forest masses, relative humidity is high near soil (surface). During dry period, transpiration remains high if roots are deep. This is increased by stomata openings. Vegetation modifies temperature and humidity of surrounding air, being water vapor transference bigger during daytime and thus relative humidity is higher than in canopy. There is a humidity gradient function of trees height; as day passes, humidity diminishes in the canopy when not yet in the soil.

Oasis effect: It is originated by contrast between a dry and a wet area, this wet zone may be natural or artificial (irrigation, very common in Spain). There is a strong relation between *potential evaporation*, or demanded by climate, and *real evapotranspiration*. Potential evaporation is the limit towards real evapotranpiration tends according to water availability in vegetation cover. But variations in real evapotranspiration are related with water availability changes, which can modify initial climatic conditions and influence potential evaporation in the zone. In this case, *Bouchet* formula shows:

$$2EP_o \leq (1\text{-}a)\, E_g \downarrow + Q_h, \qquad \text{Eq(3.45)}$$

Epo= Real evapotranspiration equal to potential evaporation, in case the only limitating factor, for a given surface, be the energy.
a= Constant
Eg ↓= global radiation
Qh= set of energy lateral phenomena (advection)

3.4.12 Climate as function of vegetation

Sensible heat flux over a forest is very low, most of incoming radiation is used as *latent energy* since transpiration of the forest system is high. Climate in a forest system depends on:

- Species
- Mass density
- Age
- Dimensions
- Grove thickness
- Soil thickness
- Relief

Climate is highly influenced by forest masses, different phenomena involving water and energy balances are affected. Fogs are more frequent around forest masses due to humidity and temperature specific conditions. Storms occurrence is the opposite, since less number are presented, compared to surroundings, because forest mass roughness slows down wind. Likewise rain is more frequent but regulated. If snow is present during winter, its melting takes longer due to differences in temperature with the surroundings and retention of snow by leaves. In many places forest creates breeze going outside during morning cause heating is less under vegetation cover and colder air from the forest

replaces hotter air outside. Bare zones, within forest or next to it, have particular features: at north side, they use reflected radiation from the forest, at west, they are colder cause use of heat to evaporate morning due. During night they are colder and freezes are frequent.

4 REMOTE SENSING (adapted and summarized from GCU and Vonder Haar)

The basic idea of this technique is to compile information about a distant object through a device (sensor) that is not in physical contact with the object itself. Its early development was closely connected to military applications but after mid 20th century it became an important tool in Earth sciences research. According to the United Nations General Assembly Resolutions and International Treaties Pertaining to the Peaceful Uses of Outer Space, *Remote Sensing* means "the sensing of the Earth's surface from space by making use of the properties of electromagnetic waves emitted, reflected or diffracted by the sensed objects, for the purpose of improving natural resources management, land use and the protection of the environment". Of course, in a broader sense, if thought about others systems acquiring distant information through a non contacting technique (e.g. medical, industrial, etc), this is also regarded as remote sensing but because of purpose, this work is focused in Earth science applications.

4.1 Sensors

Cameras and other instruments that take information about the objects and earth areas are called sensors and are transported on airplanes and artificial satellites.
Energy per unit time per wavelength (frequency, wave number) per unit solid angle crossing a unit area perpendicular to the beam is called monochromatic radiance (Vonder Haar,1995) and is the most important unit in satellite meteorology. It is detected by radiometers which collect information from narrow range of wavelengths. According to detected energy, sensors can be classified as follows:

Passives: these only measure or analyse radiant energy from the object.
Actives: in this case the sensor emits a known amount of energy (microwaves) and measures the reflected energy from the object. Radar, lidar and sonar are some examples.

According to collected information, there are two kinds:
Not forming image systems: These take point or isolated information or numerical expressions hard to visualize. It is the case for precision altimetry by laser or microwaves.
Forming image systems: These detect and analyze information from an area in each point assigning geographical coordinates. The size and distance of each point depend on the object and used sensor, this is called accuracy and resolution.

According to electromagnetic regions, there are three main strips:
Visible Near Infra-red (VNIR): comprise sensors detecting solar energy reflected by the Earth in the spectral interval from 0,4 to 2,5 μm.
Thermal infrared: in this region there are two wavelength windows, 3 to 5 μm and 8 to 14μm. The ranges between these values are absorbed by water and atmosphere gases.
Microwave: this region works with low frequencies and large wavelengths (0,1 to 100 cm). Its advantage compared with the other regions is that it can be used in all climate conditions like rain and cloudy weather.

Most of sensors register radiant or reflected electromagnetic energy. The most common electromagnetic energy is light. Remote sensing converts electromagnetic signals into analogical (photography) or digital (image) information, acquiring it in the visible and invisible like microwave and infrared. The main technique developed by remote sensing is the multispectral photography, using multispectral sensors. This allows taking photographs of the Earth from different wavelengths, generally in the visible range near to infrared. Infrared and microwaves register invisible electromagnetic energy. Heat from objects can be measured by the infrared energy they emit. Temperature variations are assessed by this mean. Infrared images are used to determine conditions of vegetation, changes in water surface temperature, damages in underground water nets and to visualize surface and underground geographical features. Radar and active sensors have the advantage of taking images through clouds, this has allowed creating radar maps, like those from Venus, which is always covered by heavy clouds, it has also been used in oceanic navigation, geology and to measure soil water content. The ESA (European Space Agency), U.S., Japan, and Russia have launched Earth watching satellites. LANDSAT satellite (first launched in 1972) has given much information about the earth; it was conceived to agriculture uses, collecting information about the land cover. Each one of its images cover about 31.000 km² showing objects of 900 km².ERS and SPOT satellites take information about continents and ocean surface, ocean streams and wind direction. Other satellites series like *NOAA*, EOS (Terra),GOES, and Meteosat are just used to watch meteorological phenomena.

4.2 Meteorological satellites

This kind of satellites has a sensor with different channels which give good space and temporal coverage. These sensors are not affected by problems related with their structure, power variations, high maintenance costs and calibration as the Earth based (radar) sensors are. Sensors placed in these satellites (polar and geostationary) are called radiometers and detect electromagnetic radiation coming from the Earth, in bands of visible spectrum (emitted by the sun) as well as the infrared (emitted by the earth). The obtained information with radiometers then must be transformed in useful physical units like temperature, radiance and albedo. Solar radiation has capacity to scatter through the space interacting with matter, this allows remote sensing taking these variations and transforming them into electromagnetic impulses. Sensors on satellites support different changes. Due to that fact, adaptations and calibration have to be made in order to get correct information about absorption and emission present in the Earth atmosphere and surface. This kind of satellites take different images:

Visible: formed by the visible light reflected towards the satellite from the Earth, the atmosphere, clouds and the ocean. These images are called panchromatic (black and white). Upper part of clouds, snow, and ice reflect well sunlight and are whiter than oceans and water bodies.

Infrared: these images represent infrared radiation emitted by the clouds, the earth and oceans. The higher the temperature the higher the emitted radiation. The grayer tones show places with higher temperature. Far from the poles, lower temperatures correspond to high clouds in the upper troposphere or lower stratosphere associated to mid latitude storms. Data and images are very important to forecasting. In this sense weather predictions within three or six hours, from low to regional scale, can be made using remote sensing.

4.3 Sensors features and data processing

When working with spatial information, the scale concept makes relation between the document and reality and tells us about the amount and quality of information that can be extracted. In case of aerial photography we can talk about scale, while in space images taken by radiometers and radars, the concept is called resolution. Resolution considers information quality in different ways, but only four are of main importance:

Spatial resolution: it is given by the *instant field of vision* (IFOV) defined as the angular section, measured in radians, in a given moment.. It is depending on the opening of the optic device of the sensor. Nevertheless when treating with spatial resolution, the distance to then ground corresponding to the angle is used to fix resolution. This distance determines the size of minimum information unit (pixel). Resolution depends on orbital height, velocity, and number of detectors. Currently, spatial resolution of sensors varies from 1m (IKONOS) to 5000m (Meteosat). Though the pixel is closely related with resolution, it is also defined by some other factors like geometry, radiation contrast between close objects, cloud and aerosol presence, etc. According to spatial resolution sensors are classified in very high, high (fine) and mid or low resolution (coarse). Improving resolution, which means enhancing accuracy for environmental and Earth science applications, is one of the most important challenges for technicians.

Spectral resolution: this one indicates number of bands and width. It depends on an optic filter device splitting the incident radiation in different spectral bands. The more number of bands and the narrower their width the higher spectral resolution for a sensor. This allows better contrast between different types of covers (GCU).

Radiometric resolution: is defined by digitalization intervals of the signal. Maximum digital levels of an image determine radiometric resolution and vary from 64, 128, 256, or 1024. Higher level means more accurate information.

Temporal resolution: this refers to coverage frequency of considered sensor. It is given by platform features (height, velocity, inclination) and sensor design (opening and observation angle).

The *optimal resolution* would be given according to a balance between these four issues and is closely related with the objective information (Chuvieco, 1996). Increasing spatial resolution means less temporal resolution and perhaps less spectral and radiometric. For

meteorological phenomena temporal resolution is required in order to follow up different phenomena. High spatial resolution would be more related to accuracy of retrieved parameters, in such a case combining data from different sensors could be useful to get more reliable information.

According to the orbit, satellites can be classified in two types:

Geostationary: the satellite goes along with the earth in its orbit. An example is METEOSAT which is situated 36.000 km high.
Sun-synchronous: the satellite goes around the earth and crosses the equator at the same local time. Examples are NOAA (833 km), LANDSAT (705km), and SPOT (803 km).
Another important satellite feature is the time resolution or the frequency it takes an image from the same place in the earth and it is very important in following up climatological events. For NOAA satellite the time resolution is 12 hours and 16 for LANDSAT. Scenes obtained from satellites have as many images as channels of the sensor (7 for LANSAT). To extract real useful information data must be post processed by computer (multispectral analysis). One advantage of these analysis is that pixels are not sorted according to only one wavelength but different spectral bands that allow differentiating zones in function to the wavelength. One common operation is pixel classification that can be visual or computed. Computed are of two kinds:
Not supervised classification: the computer does not have additional information given by the user.
Supervised Classification: the user knows previously some information about the pixel nature from field studies. These pixels are sorted by class, for the rest of the pixels; the probability of pertaining to the previous group is calculated and assignated to defined pixels. For the analysis to be done correctly, accurate information from the field has to be taken from other sources like aerial photography, thematic maps, etc. It must represent different surface spectral responses.

Classification process is made through matching spectral classes found in the image and thematic classes needed to identify, so:

Spectral classes: groups with similar spectral response called *clusters*
Thematic classes: legend, user defined categories (land use, vegetation cover, fire vulnerability etc) (GCU).

4.4 Retrieval of variables in remote sensing

4.4.1 Multi vs. Hyper spectral measurements

Sensors acquiring data from few and separated wavelengths are regarded as multi spectral (AVHRR, Landsat, Imager, SEVIRI, etc). They overlook some information about nature of studied targets since spectral response can not show a clear difference between similar materials (Shipert, 2004). This is the reason classification techniques of images are necessary for multi spectral analysis whereas hyper spectral acquired data allow in-

detail analysis of imagery without categorizing (Shipert, 2004). High number of wavelengths is not the only condition to consider a sensor as hyper spectral, besides that, bands have to cover narrow and close regions in the spectrum. Extended spectral data acquired by hyper spectral sensors gathers detailed information leading to diverse specific applications like mineral mapping, identification of vegetation species (Clark, et al 1995), soil properties (Ben-Dor, 2000), plant canopy chemistry (Aber and Martin, 1995) or vegetation stress (Merton, 1999). When comparing hyper spectral with multi spectral sensors, these kinds of uses demonstrate a clear advantage. Although we must remember that hyper spectral sensors have operational constraints related with operational features like type of platform (most of hyper spectral sensors are airborne transported) or resolution (normally higher spectral resolution means diminution in other resolution – Chuvieco, 1996-). As a result the use of one or other type of sensor would depend on specific research needs or resources and optimal spectral resolution would also depend on these needs and resources. Even if most of hyper spectral sensors are transported by aircrafts (AHS, AVIRIS, PROBE 1, HyMAP, EPS, DAIS etc), some on going projects tend to include hyper spectral sensors carried on board satellites (Hyperion on EO-1, CHIS on PROBA and FTHSI on Mighty Sat II). This will surely mean improving applications and acquisition of more and better spectral information used in diverse remote sensing techniques.

4.4.2 Temperature

Temperature has to be computed in an accurate way since it represents a key factor for important environmental research related with water and energy balances or natural threatens like desertification, fire warning, frost events, etc. (GCU). Its measurement from satellites is based on the fact that every surface emits a radiant energy proportional to the fourth exponent of its temperature (Stefan –Boltzman law). Radiometers on satellites are capable to measure energy that emits the Earth surface in different zones of the electromagnetic spectrum. This information from different bands has to be processed to get true values for physical magnitudes like temperature. Radiometers, for instance, do not get direct actual temperature values, instead they measure “radiometric temperature” which is used, after atmospheric and emmisivity corrections, to compute the real temperature values (GCU). It has to be considered that electromagnetic emissions by the Earth surface within thermal infrared region depend on their temperature and emissivity (capacity of a surface to absorb or emit energy). The radiation can also be dispersed by aerosols in its way through the atmosphere, besides that, atmosphere emits some amount of radiation depending on its temperature vertical gradient and the absorption of some of its compounds, this radiation interfere with measurements. Due to these effects, some errors can be induced in the radiometry of Earth surface. It is especially difficult to calculate when aerosols content is very high or clouds are very dense because they are dark to infrared radiation. In this case information surveyed is useless but new techniques have been developed to be able to retrieve data from such cases, e.g. hyper- frequency systems (*Johnson et al, 1994*).

A 1% variation of surface emissivity may represent a difference in temperature around 0,3 to 0,7 K. For climatology research this variation must be lower than this value (Barton, 1992).Oceans, for instance, have an emissivity near to 0,990 with low variations less than 1% between different points. That is why the ocean surface temperature is easy to find with accuracy between 0,5 to 1° C. But in emerged lands, due to surface variations, emissivity changes between 0,80 to 0,990 according to the wavelength and environmental features. To avoid mistakes estimating temperature from Earth surface, radiation and emissivity must be measured simultaneously to split temperature and emissivity effects in emitted and reflected radiation values. Radiation values taken in electromagnetic ranges corresponding to transparent and low emissive zones are known as "*atmospheric windows*". Radiation measures are done in perpendicular lines to the direction of the satellite. Each line is about 150 up to 3000 km wide and is composed by 3000 points (depending on resolution) which are swept sequence or simultaneously. Finally a digital image from the Earth surface with one value for each pixel is acquired. To obtain final values of temperature found in radiant energy, data must be transformed in luminance or apparent temperature (*brightness temperature*) once atmospheric effects have been eliminated after knowing humidity and temperature vertical profiles. When satellite radiometer takes simultaneous measurements in two spectral bands (10,5 and 11,5 μm), the survey of temperature and humidity is not needed cause combination of two bands eliminates effects. Besides that, emissivity effects of surface have to be eliminated too. For this, surface must be classified in different elements of known emissivity. Scenes taken in the studied electromagnetic spectrum are day images and show the overlaying of emitted and reflected energy, meanwhile night images only show thermal radiation emitted by land surface. When emissivity coefficients for day and night do not change considerably, surface emissivity can be deduced from two images (GCU).

Thermal infrared (TIR) bands are operated to find sea and surface temperatures and precipitable water values in remote sensing applications. TIR sensors measure radiance values which can be used to compute brightness temperature of top of atmosphere (TOA) and, although atmosphere is almost transparent in the 10.5 to 12.5 μm region, its influence is not negligible. This means, to retrieve temperature from remote sensed values some corrections of atmosphere influence have to be performed (Jimenez,2005). All approaches to calculate temperature from remote sensors are based on *Radiative Transfer Equation* (see Eq 3.27) and since it does not calculate temperature values directly but radiance values its solution is called the *inverse problem* or *retrieval problem* (Vonder Haar,1995). There are different algorithms that, mainly, use one or two channels to calculate temperature. One band methods can use the same band from different angles -*bi-angular*- or just compute temperature directly in a *single- channel* algorithm. Two bands algorithms combine values from two thermal bands in a well developed technique called *split window* (Mc Millin *et al*, 1984). More than two bands are also used in temperature retrieval algorithms (*Li et al, 1997*) but, since they are not often applied, we focus on former cases.

Single channel: Although it is normally used for only one observation angle, some other algorithms neglect angular dependence. Its application is simple because it only needs data from one thermal band (one channel effective wavelength), emissivity and

atmospheric water vapour content. Generally they perform better in low water vapour atmospheres (GCU).

Two angles: In this case also one thermal band is used but using two different viewing angles. It is based on so called *differential absorption* using nadir and forward viewing angles. The *radiative transfer equation* is applied for both angles deriving in algorithms like next proposed by *Sobrino et a*l in 1996:

$$Ts = Tn+C1\ (Tn - Tf)+C2(Tn-Tf)^2+C0+(C3+C4w)(1-\varepsilon n)+(C5+C6w)\Delta\varepsilon \qquad \text{Eq (4.1)}$$

where:

Ts, Tn and Tf are surface, nadir and forward temperatures.
C0 to C6 are bi angular coefficients
Δε is the difference between forward and nadir emissivities.
W is water vapour.

Bi angular coefficients can be found in radio sounding database, water vapour content can be as well found in satellital data (*Li et at, 2003*) or directly measured by hand photometers. Forward angles have optimal values according with sensor features (e.g. height) which output the least error (Jimenez, 2005).

Split Window Technique: In this case two bands with wavelengths in the thermal infrared window are used. It is also based on the differential absorption principle used to reduce the influence of mean brightness temperature of the atmosphere. Its solution is similar to bi angular technique but instead of nadir and forward measurements two close channels measurements are used for the same angle. For the algorithm to be applied, some assumptions have to be met (Jimenez, 2005):

- Transmissivities for two close bands in the same observation angle (53˚) are equal.
- Blackbody radiation for a given temperature, Ts, is the same for two close channels, besides that,
- In the window between 10-12,5 μm atmospheric temperatures oscillate less than 1K (Prabhakara, et at 1974) making easy the correcting process.

So the split window algorithm, for surface temperature, Ts; would look similar to the bi-angular one:

$$T\ s= T4+ !.40(T4-T5)+0.32(T4-T5)^2+0,83+(57-5w)(1-\varepsilon)-(161-30w)\Delta\varepsilon \qquad \text{Eq(4.2)}$$

where:

T4 is the radiometric temperature from band 4 (for AVHRR sensor) corresponding to 10.3-11.3μm
T5 is the radiometric temperature from band 5(for AVHRR sensor) corresponding to 11.5-12.5μm
ε is the mean spectral emissivity
Δε is the emissivity difference for 4 and 5 bands (for AVHRR sensor)
W is the atmospheric water vapour content in g/cm²

This algorithm was developed by *Sobrino and Raissouni* during 1997 and validated in situ using the AVHRR Pathfinder Oceans match –up database with estimated error of 1.3 K. Other split windows algorithms have been developed according to research demands (scale time) or sensor features, some reviews can be found in *Deepak et at*,1986 or Mc Clain, 1986.

Finally, it can be said that the use of a specific algorithm depends on factors like available radio sounding data for validation, type of sensor, resolution etc. In general the single channel algorithm may be more accurate (less than 1K) for low water vapor content atmospheres while the bi angular or the split window technique are more accurate in extended areas and therefore suitable for global scale studies. In the same sense, comparing the bi angular with the split window technique, different error sources are presented. For the split window technique errors from both bands are added while for the bi angular one the main problem arises from the fact that different angles imply geometric correction difficulties specially for heterogeneous and extended areas (Jimenez,2005).

4.4.3 Emissivity (ε)

As described by Kichoff´s law (chapter 3), it is the ratio between emitted energy by a body for a given temperature and wavelength and a perfect (theoretical) emitter (blackbody) at the same temperature and wavelength. Emissivity of land surface is determined by soil structure, soil composition, organic matter contents, moisture and vegetation cover characteristics but it is not depending on soil temperature profile or surface temperature (Van De Griend and Owen, 1993). Due to extended research about emissivity for different Earth and man made materials, its measurement itself is a common tool to assess land resources (minerals) or evaluate erosion impact (GCU). Other environmental applications normally involve energy fluxes that have to be considered in water and /or energy balances. To perform this, temperature and emissivity retrievals are needed. If we observe, temperature computing algorithms (see 4.4.2) include emissivity and difference in emissivity as input parameters. Thus, emissivity is a key factor in these cases since its accuracy is directly affecting temperature measurements. Different methods compute surface emissivity, next some of them are summarized (from Jimenez, 2005):

- *Laboratory and field measurements*: obviously these procedures are not used in remote sensing techniques. The importance of these methods is that they comprise extensive compilations of emissivity values for different materials that can be used to validate or simulate remote sensing techniques. They are compiled in data bases called *spectral libraries*, some of them like ASTER spectral library (http:/speclib.ipl.nasa.gov/) include up to 2000 spectra of natural and manmade materials.

Empirical or semi empirical relationship: previous knowledge about emissivity nature is required. Some of these methods are presented in table 4:

Table 4: Methods to retrieve emissivity in remote sensing. Adapted from Jimenez, 2005

Method name (approach)	Characteristic/Method	Author
Statistical (the radiative transfer eq is not used)	Relates log NDVI and ε	*Van de Griend and Owe, 1993*
	Average/ variance	*Stoll, 1993*
Reference band	Based on Planks law. Assuming ε constant for a multi- spectral system	Kahle et al, 1980
Normalization/TES	Use of reference ε values and max. temp to separate ε and T actual values. See pag. 42	Gillespi,1998
Alfa coefficients	ε is derived from a function of variance for different materials.	Kealy and Hook, 1993
TsRAM(Thermal shorwave Infrared radiance model)	Based on Temperature independent thermal spectral libraries	
NDVI threshold	Defined for 3 NDVI ranges. See Eq 4.3 to 4.6	Sobrino and Raissouni, 2000

- *Inversion techniques:* To be applied some approximations in spectral variations and atmospheric radiation are needed. It is a solution based on the radiative transfer equation, supposing water vapor is the main mean of transmittance (Matsumoto- Moriyama and Arai, 1994)
- *Special measurements*: these methods assume no variation in emissivity and TISI indices (temperature independent thermal spectral indices); to be applied day and night images are normally required (Becker et al, 1995), this is perhaps its main constraint.

The NDVI threshold method, mentioned in table 4 and applied in present work, is a emissivity retrieval algorithm which considers the surface as a mix of bare soil and vegetation in the image. It is based in two former models considering a geometrical approach –shape, roughness, etc- (Sobrino et al, 1990) and a TES (Temperature and Emissivity Separation) model based on the *radiative transfer equation* (see chapter 3) and developed by Gillespi et al, 1998. The method was first developed in 2000 for NOAA-AVHRR images (Sobrino and Raissouni) and two years later for high resolution sensors (e.g. DAIS). As seen in chapter 3, the NDVI (Normalized Difference Vegetation Index) is a ratio that computes contrast between red and infrared bands. While green plants have high absorption values in red and high reflection in the infra-red region, soil does not show such a high contrast. This contrast in reflectance is a practical way to find vegetation cover density and obtain emissivity values in images. There are three different kinds of pixels describing vegetation presence in the images:

- *Mix pixels*: emissivity value in this case is defined by bare soil and vegetation fractions. The total emissivity is calculated adding proportion of soil and vegetation by their correspondent emissivity values. It is also affected by surface roughness coefficient. NDVI values considered for mix pixels fluctuates between 0.2 and 0.5 and can be calculated according to:

when $0.2 \leq NDVI \leq 0.5$, then $\varepsilon = \varepsilon vi\, Pv + \varepsilon si(1-Pv)+C$ Eq (4.3)

where

εvi and εsi are soil and vegetation emissivity values
Pv is vegetation proportion, defined by Carlson and Ripley, (1997) as:

$$Pv = \left[\frac{NDVI - 0.2}{0.09} \right]^2 \quad \text{Eq (4.4)}$$

C1 is a coefficient depending on surface roughness and shape.

- *Bare soil pixels*: Reflectance of bare soils do not have a high difference between red and near infrared regions, this means low NDVI values. Emissivity of soils is not typical and depends on many factors like structure, texture, roughness, chemical composition, soil thermal and mechanical history and wave length at which emissivity is measured (Van De Griend and Owen, 1993). To apply the NDVI threshold method values under 0.2 are considered. Red reflectance and emissivity show a linear relationship used to obtain emissivity values:

when NDVI<0.2 then $\varepsilon = a_1 + b_1 \rho red$ Eq.(4.5)

where
a_1, b_1 are coefficients depending on sensor and band and are included in the ASTER spectral library
ρred is the reflectance in the red region.

Total vegetated pixels: in this case surface is entirely covered by vegetation. NDVI values above 0.5 are characteristic for dense vegetation surfaces. A constant value for emissivity is assumed:

When NDVI > 0.5, then ε = 0.990
Eq (4.6)

4.4.4 TES method *(Temperature and Emissivity Separation)*

High spectral resolution sensors provide a better approach to solve the problem about temperature and emissivity coupling (Jimenez, 2005). This technique was developed to be applied on thermal bands of ASTER sensor (Gillespi,1998) but its use can be extended to sensors with more than 4 bands in the thermal region. The *radiative transfer equation* (see eq 3.26) is applied for each thermal band using input data from upwelling surface radiance and atmospheric descending radiation. Accuracy in TES method has been found around 0.015 for emissivity and 1.5K for temperature (Hogan et al, 2000). TES method general formulation is showed:

$$\varepsilon_i = \beta_i \left[\frac{\varepsilon \min}{\min \beta_i} \right] \text{ (i=1,N)} \quad \text{Eq (4.7)}$$

where

ε_i is the emissivity for band i

β_i is the relative emissivity computed by Normalized Emissivity Method (Gillespi, 1985)

$\varepsilon \min$ is the minimum emissivity calculated from a empirical relationship which, for ASTER, is:

$\varepsilon \min = 0.994\text{-}0.687\text{MMD}^{0.737}$ Eq 4.8 where MMD (Maximum Minimum Difference) is the spectral contrast between relative emissivities.

N is the number of bands considered.

5 EVAPOTRANSPIRATION

5.1 Evaporation and evapotranspiration

Knowledge of surface waters evaporation and soil-plants evapotranspiration is a key factor for different human activities and research:

- Climate forming mechanisms and climate change modelling.
- Basic resources study (water availability).
- Development, growing and production of crops (irrigation).
- Development and growing of forest masses.
- Disaster warning.

The term evapotranspiration is used in hydrology and climatology and normally computes the volume of water loss from a vegetated surface while the energy used in the same process is known as *latent heat flux*. Both terms refers to the same process but from different approaches. Basically evaporation and evapotranspiration terms refer to the same mechanism only differing by the surfaces they take place from (Brasa, 1997). In nature they happen simultaneously and their separation is not easy to perform, therefore both terms are usually computed as a single one: evapotranspiration. Evaporation is a diffusion process where water becomes gas (water vapour) and returns to the atmosphere. It happens when enough energy is supplied to liquid water increasing rate of movement (kinetic energy) between its particles . It is also depending on atmospheric conditions (e.g. radiation, wind speed, humidity, pressure, etc) and surface characteristics (roughness). Source surfaces can be water bodies, ground (diffusion) or vegetation (diffusion and transpiration). *Diffusion* process of *evaporation*, Ev, is expressed in Eq. 5.1 by Ficks law:

$$Ev = K_E U(e_s - e_a) \qquad \text{Eq (5.1)}$$

where:

K_E is the water vapor transport vertical efficiency,
U is the generated turbulence by wind
$(e_s - e_a)$ is the water vapor deficit between surface and air.

Transpiration is the loss of water through the vascular system of plants in a physic-metabolic process. It comprises water absorption by roots and transport (along with dissolved ions) by xylem to leaves where according to physiological demand is released to the atmosphere (partial pressure difference diffusion) while CO_2 is uptaken. The diffusive flux in leaves depends on openings (stomata) surface area, water flux density and transport coefficient, which is function of temperature. The bigger difference between free surface water and plants is that plants can physiologically regulate water loss until some extent by controlling stomata action. External factors like light, humidity and water content rule this controlling function. When water is released to the

atmosphere, pressure drops and allows water movement by osmosis. This movement (upward) creates a pressure gradient between soil and roots (Lampinen et al, 2003) that allows water uptake for plants. The water movement from soil, through plants, to the atmosphere is an important mechanism in water studies since, along with precipitation, they represent the main components in the water balance. A detailed follow-up of the water movement in vegetation was presented in the soil-plant atmosphere continuum (SPAC) concept by Philip, 1966.

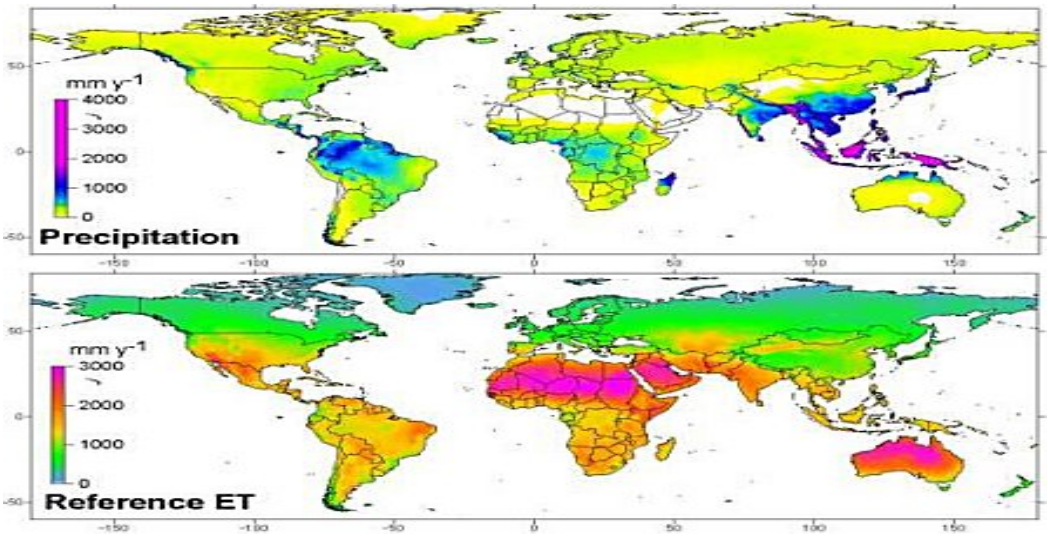

Figure 6. Global annual precipitation and potential evapotranspiration. Source: International Water Management Institute, 2001.

Potential(ETP), Reference and actual Evapotranspiration
ETP is a concept introduced by Thornwaite (1948) which defines the maximum amount of water that can be evaporated from a vegetated surface with optimal development and no water limitations (field capacity).

Reference evapotranspiration (ET_0). It is similar to ETP concept but it introduces a standardized crop with known parameters. Height, shadowed surface, crop resistance and albedo are some of these parameters. Grass (Doorenbos and Pruitt, 1977) and alfalfa (Jensen et al, 1990) are conventional crops used to define it. The water demand for crops changes through phenological stages being higher during growing phases. The process of transpiration dominates over evaporation as the leaf area index grows (Santa Olalla, et al, 1993).

The ET_0 is a necessary concept to compute the crop evapotranspiration, Et_c, which depends on a specific dimensionless coefficient, k_c, for different crops, and is expressed:

$$Et_c = ET_0 k_c \qquad \text{Eq(5.2)}$$

Where the crop coefficient, k_c, is a empirical relationship depending on crop type, phonological stage, climate, soil water availability, even cultivation techniques and mainly water supply - rain or irrigation - frequency (Doorenbos and Pruitt, 1977; Hupet et al, 2001).

Logically crops or vegetation are not always on optimal or theoretical conditions and real evapotranspiration values differ from definitions above presented. Because of that fact, the concept of actual evapotranspiration, AET, is needed. As indicated, it computes the true amount of water loss through the soil-plant system. In the end, all definitions presented stand for models related with optimal water supply, i.e. the ETP concept, and since the actual evapotranspiration is really dependent on specific conditions (climatic, soil water, species, etc), generalizations are hard to make. In consequence EAT measurement are limited to direct estimations done in tanks (lysimeters) with natural restrictions in scale.

Methods estimating water contents in soil can also be used to compute ET. This can be performed through *capacitance sounds* which measure humidity fraction to some fixed depth but in any case these values would be only useful to estimate evapotranspiration indirectly (Weinzettel et al, 2001).

5.2 Evaporation and ET Measurements

5.2.1 Indirect methods to estimate Evaporation

Evaporation can be analyzed in different ways. Vapor tension in equilibrium with liquid water (saturated vapor tension), only depends on temperature. Consequently different formulas are based on this relationship, here Alt`s formula is presented:

$$e\,(T) = 6{,}1070[1 + \sqrt{2}\,\sin(T/3)]^{8.827} \qquad \text{Eq (5.3)}$$

where

e= equilibrium vapor tension (hPa)
T=temperature (ºC)
T/3= angular degrees

5.2.2 Direct methods to estimate Evaporation

Atmometers:

- Livingstone: a hollow porcelain porous sphere joint by a tube to a graded deposit containing distilled water

- Piche it is a graded inverted pipette, it contains water and is placed over an absorbent paper of 13cm^2. It is also useful to calculate evapotranspiration since the advection term from *Penmans* equation can be found.
- Evaporation pans: they are useful to calculate evaporation and find a term to calculate evapotranspiration:

Type A: these are cylindrical with a standard diameter of 12 m and 0,25m depth. They are placed 5 to 10 cm over the surface and have a graded scale allowing more than one register a day.

Underground tanks: can be cylindrical with conic bottom (MWO suggested). They have a pipette to measure water level. There are other models with rectangular or square section and are placed 5 to 10 cm over surface.

Evaporation tanks can also be used to calculate potential evapotranspiration and real maximum evapotranspiration (for crops). Though all evaporation tanks are highly sensible to advection and may be interfered by insects or birds.Their use is important to quantify evapotranspiration when transformation coefficients are known, these are computed as a function of season:

$$ETPc = \alpha d \, Ed \qquad Eq(5.4)$$

where

ETPc= climatic potential evapotranspiration
αd=transformation empirical coefficient (for the tank)
Ed = evaporation from the pan.

The surroundings of evaporation tanks influences measuring, for instance, class A have significant differences when grass is present (*αd=0,3)* or with bare soil (*αd=0,8)*. If deposits are square, controlled evaporation is very close to ETPc.

5.3 Evapotranspiration measurement (local scale methods)

5.3.1 Lysimeters

Evapotransporimeters: are lysimeters used to measure real maximum ET from a dense vegetation cover with unlimited water source all the time. They are formed by a prism or bucket with a soil content where water movements are controlled. Water balance is assessed:

$$AET = P + I - D \qquad Eq\ (5.5)$$

where

AET= actual evapotranspiration
P= precipitation
I= water supply (irrigation)

D= loses as drainage

P,I,D can be measured easily if field capacity is kept with irrigation when needed. Maximum real evaporation (AETM) can be studied if vegetation is enough and dense.

Lysimeters, lysimetric boxes: here the prism of controlled soil is used to measure AET in crops, to follow fertilizers development, plant nutrition, mineral salts movement, etc. Weigh lysimeters (mounted on a scale) can detect changes in soil water contents, so:
ΔS= P+I-AET, (AET=P+I ΔS), where
ΔS=water content change in soil.
With these lysimeters AET can be measured continuously in any vegetation cover.

Other local methods to estimate evapotranspiration use equations which input meteorological variables that can be summarized in three different types shoed in table 5 (adapted from Jensen, et al 1990):

Table 5. ET models at local scale (Adapted from Jensen,1990)

Method	*Climate*						*General Equation*
	Humid			*Dry (arid)*			
Temperature							
	R	*S*	*RMSE*	*R*	*S*	*RMSE*	
Blaney Criddle	*6*	*+17*	*1,.0*	*4*	*-16*	*1,3*	ETo = p (0.46 Tm + 8)
Thorntwaite	*5*	*-4*	*0,9*	*7*	*-40*	*2,4*	*Et=1,6(10Ta / I)* ^{a}
Turc	*2*	*+5*	*0,6*	*5*	*-30*	*1,9*	$ETo = a_t 0.013 \frac{Tm}{Tm+15} \frac{23.88Rs+50}{\lambda}$
Radiation							
Priestley Taylor	*3*	*-3*	*0,7*	*6*	*-30*	*1,9*	$ET=\alpha\frac{\Delta}{\Delta+\gamma}(Rn-G)$
FAO 24 radiation	*4*	*+22*	*0,8*	*2*	*+6*	*0,6*	$ETo = a + b\left[\frac{\Delta}{\Delta+\gamma} Rs\right]$
Tank method	*7*	+14	*1.3*	*3*	+21	*1.5*	

where

R is ranking, S is over/ under estimation between 11 lysimeters(%)
RMSE is the root mean square error.:
ETo = Reference monthly mean crop evapotranspiration (mm/day).
T mean = mean daily temperature (°C)
p = mean daily annual daytime hours (%)
Ta is the monthly mean air temperature
I is the annual heat index
a, in Thornwate, is a exponential depending on the annual heat index (latitude)
a_t is a coefficient based in humidity values
Rs is the solar radiation (MJm $^{-2}$ day^{-1})
λ is the latent heat of vaporization (MJ kg^{-1})

ά is a coefficient depending of climate(wind, humidityregimes) with a value of 1,26 for most of condition (Itier, 1996).

Δ represents the slope of the saturation vapor pressure- temperature curve (PaK^{-1})

λ is the psychometric constant(PaK^{-1})

Rn is the net radiation(J $m^{-2}s^{-1}$)

G is the soil heat flux (J $m^{-2}s^{-1}$)

a and ,b in FAO 24, are coefficients depending on saturation in daily mean relative humidity and mean daily wind speed respectively.

FAO Penman-Monteith Method

This method, ranked number 1 in the comparative study shown in table 5, is a combination of methods using temperature and radiation and has been chosen by the FAO as the reference method (56PM) since it performs well in different types of climates. Jensen reported misestimating values of +4 and -1% for humid and dry climates respectively. For this reason and due to succesful applications found in other places and for different types of climates the method is considered the most accurate one (Qui et al, 2002). Despite this method is still regarded as the best one between local methods, its application is considered difficult because the high input of meteorological data demanded for its performance (Dingman, 1994). Nevertheless the method has been adapted to specific climates and crops and where enough data is available, is it recommended to be used. Based on a method proposed by Penman in 1948, it introduces aerodynamic and bulk surface resistance (Allen, 1998) terms:

$$\lambda ET = \frac{\Delta(Rn - G) + \rho_a c_p \dfrac{e_s - e_a}{r_a}}{\Delta + \gamma(1 + \dfrac{r_s}{r_a})} \qquad \text{Eq (5.6)}$$

where

λ is the latent heat of vaporization ($J\ kg^{-1}$)

R_n is the net radiation ($Jm^{-2}s^{-1}$),

G is the soil heat flux($Jm^{-2}s^{-1}$),

(e_s - e_a) is vapour pressure deficit of air, between saturated and actual in Pa,

ρ_a is air density (kg/m^3),

c_p is the specific heat of the air($Jkg^{-1}K^{-1}$),

Δ represents the slope of the saturation vapour pressure- temperature curve (PaK^{-1}),

λ is the psychometric constant(PaK^{-1})

and r_s and r_a are the (bulk) surface and aerodynamic resistances(m/s).

5.3.2 Evapotranspiration measurement (regional methods)

As seen before AET can be measured directly but its measurement is limited to operational capacity of meteorological stations containing lysimeters (local scale) or, at

least, enough and reliable meteorological data. Lysimetric stations are expensive and demand some technical support making AET measurements really low represented in coverage. Anyway, if meteorological data or lysimetric stations are available, the AET is still limited to local applications. Nowadays climate and hydrological research demand consistent methods to extend ET in time and space to regional scales since local phenomena are not isolated and may affect larger areas but it is difficult to establish exact relationships between different scales (extrapolation). Remote sensing applications tend to solve these limitations by measurements covering regional to global scales (Caselles et al, 1993). Methods to compute ET using remote sensed information could be classified in semi-empirical, analytic or simulation algorithms (Caselles, et al 1993). Sanchez, 1998, proposed a practical classification of mentioned methods in four groups:

Surface energy balance based methods*:*
The fate of in coming energy can be split in three main portions: one part returning to the atmosphere as Earth radiation, another, the sensible heat, used in heat transference between matter and one more used in the ET process known as the latent heat. The latter portion is difficult to be exactly computed and since the other two are easier to retrieve through remote sensed information, the estimation of latent heat can be performed in a residual method when sensible heat and Earth radiation, besides the incoming radiation, are known (Choudhury, 1995).General expression is presented:

$$\lambda ET = Rn - G - H \qquad \text{Eq (5.7)}$$

where

λ ET is the latent heat flux with λ as the latent heat of vaporization (2,45MJ kg^{-1})
Rn is the net radaiation
G is the ground heat flux and
H is the sensible heat flux.

S*urface temperature based models: residual method*
When evapotranspiration is taking place part of the incoming energy is been used and surface temperature decreases in consequence. Vegetation covers have different features affecting evapotranspiration process, i.e. not all vegetated surfaces make use of the same amount of energy to evaporate the same amount of water. Factors like topography, wind, vegetation species affect the fraction of energy used in the process. As a result, surface temperature is variable and indicates the distribution of available energy used for ET by different vegetation covers. Therefore surface temperature can be used to derive ET measurements from remote sensed information. Also in this case the ET measurement is found by the residual method based on daily net radiation *(Rnd, expressed in mm/d)* and air and ground temperature difference *(Ts-Ta)* around noon. The general method was presented by *Jackson et al in 1977:*

$$ETd = Rnd - B\,(Ts - Ta) \qquad \text{Eq (5.8)}$$

where

B is an empirical constant

Compared to former method, this one omits the ground heat flux (for daily measurements) and computes sensible heat based on air and surface temperature difference.

Other methods are based on the same model but introducing more empirical constants or specifications for the crop (Caselles et al, 1998) to be able to validate it for specific areas. These constants are based on regional conditions characterizing an area using ground based measurements. For instance, the model has been applied using NOAA-AVHRR images and meteorological data from 17 stations distributed over France in a campaign conducted from 1985 to 1987. In a similar campaign NOAA-AVHRR and METEOSAT images were used in Senegal (Kerr, et al, 1989).

5.4 Evapotranspiration and vegetation relationship based models

High contrast in vegetation reflectivity between red and near infrared bands is broadly used to derive vegetation indices (see chapter 3). These indices, normally presented as ratios between visible and thermal infrared channels, are useful to get information about vegetation cover, density, productivity, stage, etc and can be used to establish relationships with water demand by crops (Kerr et al, 1989). Choudhury (1995) proposed a model to compute (AET) using vegetation cover (derived from SAVI index) and ETp:

$$AET=ETpfc \qquad \text{Eq(5.9)}$$

where

fc is the green vegetation cover fraction, found using SAVI index.

Another method, applied in dry regions where ET exceeds precipitation, computes AET from remote sensed images using NDVI index and potential ET values (Gutman et al, 1995).

5.4.1 Vegetation indices and surface temperature relationship based models

Vegetation masses influences climate and normally regulate temperature showing lower values as vegetation areas increase in density and size, expressed in different words, denser and larger vegetation covers use more energy (latent heat) to evapotranspirate water, leaving less available energy to “heat up the air” (sensible heat) with consequent temperature variations (Nemani et al, 1993). These variations in surface temperatures between different vegetation covers combined with vegetation indices (e.g. NDVI) can be used to compute ET (Choudhury, 1994, Nemani et al, 1993). Vegetation indices and surface temperature acquired from remote sensed information have been also used as water stress in vegetation and related to water availability and evapotranspiration. A use of this relationship, known as *Crop Water Stress Index* (CWSI) is proposed by Jackson et al, 1981:

$$\frac{AET}{ETp} = \frac{Ts - Ts\max}{Ts\min - Ts\max} = 1 - CWSI \qquad \text{Eq(5.10)}$$

where

AET is actual ET

ETp is potential ET

Ts is surface temperature

Ts max and Ts min are the maximum and minimum temperature in the studied area.

This method is really useful and accurate when ETp data are available from conventional methods but has a limitation since it can only be applied for areas completely covered by vegetation. A modification of the model was introduced (Moran et al, 1994) to be able to apply it to extended areas since most of real cases extended areas have different vegetation densities and mixture between bare soil and vegetation. The method has a graphical representation of the relationship (term fc used in Eq 5.9) between the difference in temperatures from air and surface and NDVI. The result of this plotting is normally a trapezoid, from which the method take it name (Vegetation Index/Temperature Trapezoid-VIT-) where lower vertices correspond to bare soils (humid to wet) and the upper vertices stand for vegetated surfaces (from well watered to water stressed). The VIT allows calculation of another index, the *Water Deficit Index* – WDI-(Desbois et at, 1997) which can be used with different density covers:

$$\frac{AET}{ETp} = \frac{(T_s - T_a) - (T_s - T_a)_{dry}}{(T_s - T_a)_{wet} - (T_s - T_a)_{dry}} = \frac{BC}{AB} = 1 - WD \qquad \text{Eq (5.11)}$$

where

AET and ETp are actual and potential ET

$(T_s - T_a)$ surface and air temperature difference for every pixel.

$(T_s - T_a)_{wet}$ surface and air temperature difference for every pixel in wet areas (vegetated and non vegetated surfaces)

$(T_s - T_a)_{dry}$ surface and air temperature difference for every pixel in dry areas (vegetated and non vegetated surfaces)

BC and AB are distances found in the trapezoid formed by wet and dry areas in vegetated and non vegetated surfaces .

6 DATA

6.1 Data collection and sensors features

Sensors used in present work are considered as *passives,* since they just register the energy emitted from the observed objective, the Earth surface. The output of each sensor is an electrical potential difference which is proportional to the energy striking the sensor per time unit. When the area of the sensor, the spectral response function of the optics and the field of view of the instrument are considered, the output voltage is proportional to the radiance of the scene that the instrument is covering. The analogue voltage is digitized for transmission to the ground. (Kidder and Vonder Haar). To apply S SEBI model, the one used in present document, acquired images must include water saturated and dry surface areas, as a basic condition to calculate the evaporative fraction, and a cloud free scene as a condition to calculate (actual) albedo for different surfaces. Image acquisition included airborne and satellitel. Data collection was performed during summer (July 18 2004) with steady atmospheric conditions. Image characteristics like size, acquisition format and map information are presented in table 6:

Table 6: Image characteristics

NOAA	ASTER	AHS
Projection: Geographic Lat / Lon	Projection: UTM Zone 30 N	Projection: UTM Zone 30 N
Pixel: 0.0166667 degrees	Pixel: 15m ; 90m (Temp)	Pixel: ≈5,9m
Datum: WGS 84	Datum: WGS 84	Datum: WGS 84
UL Geo: 9°58`60.00``W 43° 58´60´´ N	UL Geo: 2° 21`38,74`` W 39°23`14.6´´N Map:555049.8 W 4359961.7N	UL Geo: 2° 21`38,74`` W 39°23`14.6´´N Map:555049.8 W 4359961.7N
Image size: 901x541	Imagesize:4980x4200,830x700(T)	Imagesize:750x2472
Recording format:(Floating point) BSQ -Band sequential -	Recording format:(Floating point) BSQ -Band sequential -	Recording format:(Floating point) BSQ -Band sequential -

6.1.1 Airborne data (AHS)

The Advanced Hyperspectral Scanner, AHS (Daedalus Enterprise Inc., WA, USA) sensor was transported by a CASA 212 aircraft operated by INTA, Spain (Instituto Nacional de Técnica Aeroespacial) at approximately 1000m high. The flight lines followed the sun direction to reduce angular effects in the images.

Line 1	579592E 4327176N
	574817E 4321401N
Line2	580092E 4326751N
	575317E 4320976N
Line 3	580562E 4326401N
	575792E 4320601N
Line 4	573867E 4329301N
	581592E 4322951N
Line 5	572742E 4327951N
	580492E 4321576N

Line 6	571617E 4326601N
	579367E 4320251N
Line 7	581142E 4324701N
	573742E 4323301N
Line 8	572742E 4327951N
	580492E 4321576N

Time of flight: 10:50 (18-07-2004).

This sensor gets information through 80 bands (in table 8) in four ports (VIS, NIR,SWIR,MWIR and LWIR) from 0,43 to 12,5 μm, but only ten of that pertaining to thermal spectrum (8,40 to 12,45 μm) and 20 to the visible and near infrared (0,440 – 1,0 μm) are of interest for present work. Image acquisition is made through a rotating mirror in a mechanical sweeping known as *whiskbroom,* getting information in lines perpendicular to platform (aircraft) scrolling. Thus, one sweeping line corresponds to a pixel line. The instantaneous field of view (IFOV) and platform height determine spatial resolution and the total angular view field (FOV) of the mirror determines image and sweeping line width. Next, flight parameters and technical specifications for AHS sensor are presented in table 7:

Table 7**. AHS** flight parameters.

FOV – IFOV	90º & 2.5 mrad
Flight height	975 and 2745m
GIFOV(ground-projected IFOV)Nadir	2.5 m and 6.9 m
Swath width	1961 m and 5491m
Scan speed	35 rps / 12.5 rps
Inertial Navigation System	Applanix POS/AV 410
Black Body thermal reference	15º C and 55º C

Source: SPARC campaign 2004.

AHS technical specifications Digitized field of view…….. 86°
Scan rates (scans/sec)…… 25, 16.7, 12.5,8.3, 6.25 (operator selectable)
Roll correction…….± 15° of roll (automatic)
Power requirements……28± 3 VDC, 50 amps continuous
Digitisation precision…….. 12-bit Data Words ± 1 least significant bit
Data recording: 8 mm Exabyte Mammoth – 20 Gbyte capacity
Record time per tape: 160 minutes minimum using recommended cartridge
Image Display: 9" CRT (continuous moving window, RS-170/CCIR output)
750 samples per line.

Table 8 AHS spectral bands

Optical Port	*Number of bands*	*Spectral region*	*Band width*
VIS and NIR	20	430 to 1030 nm	30 nm
NIR	1	1.550 to 1.750 μm	200 nm
NIR	42	1.994 to 2.540 μm	13 nm
NIR	7	3.3 to 5.4 μm	300 nm
LWIR	10	8.20 to 12.7 μm	400 nm

Source: *SPARC campaign 2004 home page*

6.1.2 Satellite data (NOAA and TERRA)

- NOAA 16

NOAA 16 satellite transports *AVHRR* sensor in a circular sun – synchronous orbit at 833 Km altitude and flew over the study area at 11:12 during the test day (18-07-2004). The AVHRR has an elliptical scan mirror, with a major axis of 29, 46 cm and minor axis of 20,96 cm, rotating at 360 rpm. Due to NOAA series satellites move at a rate of about 392 km/min, the distance between successive scan lines at the sub satellite point is about 1,1 km. This determines the spatial resolution. The output of the AVHRR sensor is an analogue voltage that is digitalized for transmission to the ground with 10 bits capacity to represent the radiance for each pixel (Kidder and Vonder Haar). AVHRR sensor onboard NOAA 16 has 4 bands showed in table 9 (one in the visible, one in the near infrared and two in the thermal):

Table 9. Noaa´s *AVHRR Bands*

Band	***Spectral interval µm***	***Spatial Resolution Km***	***Uses***
B1	0,58-0,68	1,1	Clouds, snow, ice monitoring
B2	0,72-1,1	1,1	Land cover and water bodies. Agriculture
B3	10,3-11,3	1,1	Ocean surface temperature, soil humidity
B4	11,5-12,5	1,1	Ocean surface temperature, soil humidity

Source: *Fusco and Muirheadm (1987)*

Data acquisition may be in four different ways:
- *APT (Automatic Picture Transmission):* transmitted data can be acquired in real time by omni directional antennas. Though this mode has a low spatial resolution (4km) it can get data through simple and low cost arrangements (e.g. sea platforms).
-*HRPT (High Resolution Picture Transmission):* transmitted data is acquired to high resolution antennas (1,1 Km) with limited reach but commonly used because of almost worldwide coverage (this was the case in present work).
-*LAC (Local area Coverage):* full resolution data (1,1 Km) are registered onboard the satellite and then transmitted to the land receiving stations and is used when HRTP station are not available.
-*GAC (Global Area Coverage)*: data are re-calculated, before transmission, onboard the satellite using four out of five pixels (mean average) by line and one out of three lines within images. This is made in 4km spatial resolution.

Next, georreferencing and map information for Noaa images is presented:

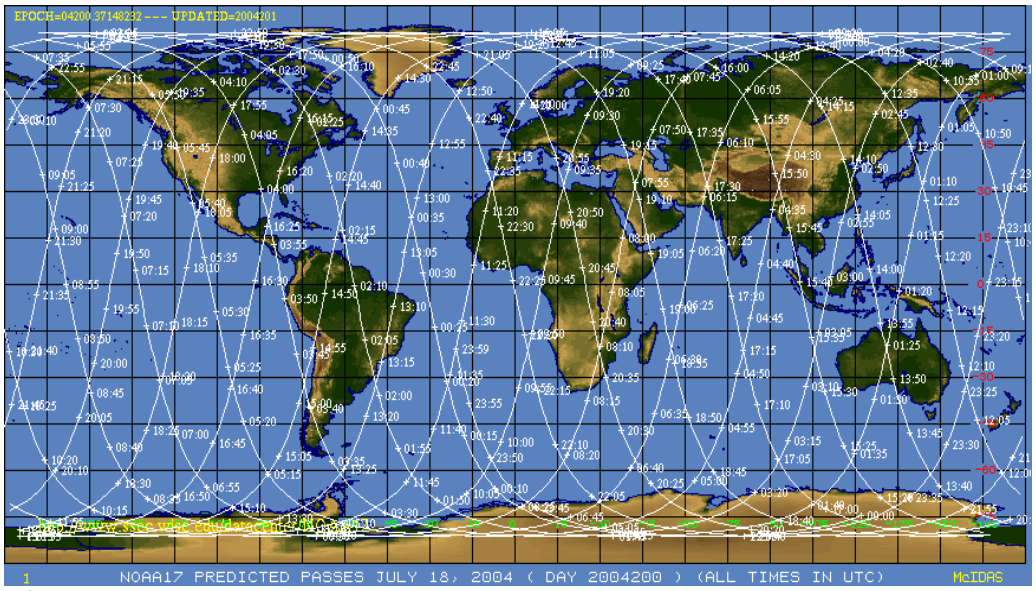

Figure 7 *Noaa overpass,* Source: *NASA*

For detailed information about AVHRR orbit tracks see http://www.noaa.gov/.

Table 10. Noaa satellite features

NOAA (16) Characteristics	
Main body	4.2m (13.75 ft) long, 1.88m (6.2 ft) diameter
Solar array	2.73m (8.96 ft) by 6.14m (20.16 ft)
Launch vehicle	Lockheed Martin Titan II
Launch place	May 13, 1998 Vandenburg Air Force Base, CA
Orbital information	Type: sun synchronous Altitude: 833 km Period: 101.2 minutes Inclination: 98.70 degrees
Weight at liftoff	2231.7 kg (4920 pounds) including 756.7 kg of expendable fuel
Sensors	*Advanced Very High Resolution Radiometer (AVHRR/3)- used in present work-* Advanced Microwave Sounding Unit-A (AMSU-A) Advanced Microwave Sounding Unit-B (AMSU-B) High Resolution Infrared Radiation Sounder (HIRS/3

http://www2.ncdc.noaa.gov

Platforms such as the Advanced Very High Resolution Radiometer (AVHRR) have proved efficient at mapping vegetation at global and continental scales (Tucker *et al.*, 1985; Goward *et al.*, 1985; Justice *et al.*, 1985; Kogan, 1991; Nogi *et al.*, 1993; Kaufman *et al.*, 1992). For continental mapping of vegetation NOAA data have been used to calculate the Global (or Green) Vegetation Index (GVI). The GVI, with its 4 km pixels,

can be applied to forest ecosystem modelling and atmospheric emissions of vegetation at a global scale (Gaston *et al.*, 1997).

Terra´s ASTER

The Advanced *Spaceborne Thermal Emission and Reflection Radiometer, ASTER,* sensor was built in Japan for the Ministry of Economy, Trade and Industry (METI). A joint United States/Japan Science Team is responsible for instrument and operates onboard TERRA platform at 705 km height in a near polar orbit once every 98 minutes. The study day (18-07- 2004) TERRA spacecraft descended southward across Barrax at 11:00 local time. ASTER collection of data is not continuous, it collects an average of 8 minutes of data per orbit with high spatial resolution (15 to 90m). ASTER is complementing the more frequent return period but lower-spatial-resolution sensor MODIS.

All three ASTER telescopes (VNIR, SWIR, and TIR) are pointable in the cross track direction. With 14 different bands ranging from visible to thermal infrared light, its high spatial resolution, its shifting angular views, ASTER sensor is useful to create detailed maps of land surface temperature, emissivity, reflectance and elevation as well as generating stereoscopic images and detailed terrain height models. (source: http://asterweb.jpl.nasa.gov/)

Table 11. ASTER spectral bands arrangement

Subsystem	Band No.	Spectral Range (μm)	Absolute Accuracy (σ)	Spatial Resolution	Signal Quantization Levels
VNIR	1 2 3N 3B	0.52 - 0.60 0.63 - 0.69 0.78 - 0.86 0.78 - 0.86	≤± 4 %	15 m	8 bits
SWIR	4 5 6 7 8 9	1.600 - 1.700 2.145 - 2.185 2.185 - 2.225 2.235 - 2.285 2.295 - 2.365 2.360 - 2.430	≤± 4 %	30 m	8 bits
TIR	10 11 12 13 14	8.125 -8.475 8.475 -8.825 8.925-9.275 10.25-10.95 10.95-11.65	≤ 3K (200-240K) ≤ 2 K (240-270K) ≤ 1K (270-340K) ≤ 2K (340-370K)	90 m	12 bits

Source: SPARC, 2004

Table 12 *ASTER System Baseline Performance Requirements*

Swath Width	60 Kms
Total Cross-Track Coverage	± 116 to ± 318 Kms
Stereo Base-to-Height Ratio	0.6 (along-track)
Modulation Transfer Frequency	0.25 (cross-track) 0.20 (along-track)
Band-to-Band Registration	0.2 pixels (intra-telescope) 0.3 pixels (inter-telescope)

Duty Cycle	8 % (VNIR & SWIR) 16 % (TIR)
Peak Data Rate	89.2 Mbps
Mass	406 Kgs
Peak Power	726 W

Source: http://edcdaac.usgs.gov/aster/asteroverview.asp

6.1.3 Land based data

The University of Castilla-La Mancha manages the agro-meteorological stations in the study area of Barrax. Two stations were used to compute evapotranspiration in Barrax field:
Tiesas-Anchor Station (39º 02' 31" N; 2º 04' 55" W)
Tiesas-Lysimeter Station (39º 03' 30" N; 2º 05' 24" W)

Both are connected by modem with the central computer at the Institute for Regional Development in Albacete and compile and store automatic data for later treatment, as well as being accessible in real time. Measurements are done by all sensors every 30 seconds and are stored every 10 minutes.
The following measurements are available from each station:

Tiesas-Anchor Station:

Anemometer (10m) Soil moisture (0,90m)
Wind direction (10m) Atmospheric pressure
Temperature and relative humidity (10m) Evaporation
Anemometer (2m) Precipitation
Temperature and relative humidity (2m) Reflected short radiation
Temperature (0,5m) Shortwavelength net radiation
Shortwavelength incident radiation *
Soil temperature (0,50m)
*Long wavelength incident radiation**
Soil thermal flux (0,05m)
Long wavelength reflected radiation
Soil thermal flux (0,10m)
Long wavelength net radiation
Soil thermal flux (0,20m)
Soil temperature (0,10m)
Soil thermal flux (0,30m)
Soil temperature (0,25m)
Soil moisture (0,30m)
Soil temperature (0,35m)
Soil moisture (0,60m)
* Used in model

Tiesas-lysimeter Station:

Pluviometer
Temperature and Relative humidity (2m)
Temperature Sensor
Relative humidity Sensor
Piranometer (2m)
Radiometer neto (2m)
Anemometer (2m)
Reflectometer for water soil content
Evaporimetric bucket
CR10 Data logger
Reference Lysimeter
Herbal Crop Lysimeter
Ligneous Crop Lysimeter

7 METHODOLOGY

Despite the fact that ET is a complex mechanism happening at land, it involves energy exchange mechanisms verified up and downward the plant/soil system itself. Once incoming energy from sun reaches the Earth, it gets a balanced state thorough transmission, reflection and absorption. Available energy is transferred to air (sensible heat) and subsurface (geothermic flux) and the remaining part, known as latent heat flux, is absorbed during water phase change to vapour and accounts for the consumed energy by the ET process. Since latent heat can not be retrieved directly by remote sensed data, then it has to be derived as the residual term of the Earth energy balance equation. Most of models to retrieve ET from remote sensed data are based in this principle. Model used in present work is based on a simplification of this relationship between radiation and energy fluxes. Visualization of all the input parameters and processes within of the model can be seen by the end of this chapter in figure 8.

7.1 Model

The *S SEBI* (Simplified Energy Balance Index) was first proposed and tested by G J Roerink, Z Su and M Menenti in Tuscany campaign at Piano di Rosa area during August 1997. The proposed algorithm is based on energy balance equation and Evaporative fraction to derive daily evapotranspiration (ETd). The equation (Eq 7.1) is presented as:

$$ET = \frac{1}{L}\Lambda(Rn - G) \qquad \text{Eq (7.1)}$$

where

L is the latent heat of vaporization (2,45 $MJkg^{-1}$)
Λ is the instantaneous evaporative fraction (dimensionless)
Rn is the net radiation derived from $R_{ni,}$ the instantaneous net radiation flux (Wm^{-2})
G is the soil heat flux derived from $G_{i,}$ the instantaneous soil heat flux (Wm^{-2})

The instantaneous net radiation flux can be obtained through the radiation balance equation according to Hurtado and Sobrino (2001):

$$R_{ni} = (1 - \alpha)\, R_{c\lambda\downarrow} + \varepsilon\, R_{g\lambda\downarrow} - \varepsilon\delta T_S^4 \qquad \text{Eq (7.2)}$$

where

α is the albedo
$R_{c\lambda\downarrow}$ is the incoming shortwave radiation (Wm^{-2})
$R_{g\lambda\downarrow}$ is the incoming long wave radiation (Wm^{-2})
δ ($Wm^{-2}\ K^{-4}$) is the Stefan Boltzman constant 5.67 x 10^{-8} W $m^{-2}\ K^{-4}$
ε is the surface emissivity
T_S is the surface temperature (K)

For different sensors, red and near infrared bands are used to calculate *Albedo*, so:

AVHRR: red band, B1, (0,58-0,68) and near infrared,B2, (0,72-1,1 μm) average
ASTER: Very Near Infra red Bands, B1 VNIR 0.52 - 0.60 ; B2 VNIR 0.63 - 0.69 ;B3 VNIR 0.76 - 0.86 μm average.

AHS: applying a weighting factor between bands in the visible and near infrared region (0,430-1,030 μm)

The *NDVI* (Normalized Vegetation Index, *Rouse et al 1974)* threshold method (Sobrino and Raissouni, 2000) was used to calculate surface emissivity, ε, in ASTER and AVHRR, so:

for *ASTER* (bands 10 to 14 emissivity average) :

NDVI<0.2:

$\varepsilon 10 = -0.298 b2 + 0.987$ Eq (7.3)
$\varepsilon 11 = -0.251 b2 + 0.984$ Eq (7.4)
$\varepsilon 12 = -0{,}259 b2 + 0.978$ Eq (7.5)
$\varepsilon 13 = -0.041 b2 + 0.977$ Eq (7.6)
$\varepsilon 14 = -0.038 b2 + 0.977$ Eq (7.7)

where

b2 is Aster band 2 in the near infrared (0,6610 μm)

0,2≤ NDVI ≤ 0,5:

$\varepsilon 10 = 0.973 + 0.019 Pv$ Eq (7.8)
$\varepsilon 11 = 0.974 + 0.016 Pv$ Eq (7.9)
$\varepsilon 12 = 0.972 + 0.018 Pv$ Eq (7.10)
$\varepsilon 13 = 0.0984 + 0.05 Pv$ Eq (7.11)
$\varepsilon 14 = 0.986 + 0.004 Pv$ Eq (7.12)

where

Pv is the vegetation cover (Carlson and Ripley, 1997):

$$Pv = \frac{(NDVI - 0.2)^2}{0.09}$$ Eq (7.13)

NDVI>05; E=0.990 Eq (7.14)

For *AVHRR (NOAA):*

NDVI<0.2

$\varepsilon = 0.980-0.042b1$ Eq (7.15)

where b1 is AVHRR band 1 reflectivity (0.58-0.68 μm)

$0.2 \leq NDVI \leq 0.5$

$\varepsilon = 0.971+0.018Pv$ Eq (7.16)

where Pv is the vegetation proportion (see Eq 6.13)

NDVI > 0.5

$\varepsilon = 0.985+C$ Eq (7.17)

where C= 0.005

and finally emissivity for AHS which is measured directly by the sensor as the average of bands 75 (9.80 μm) to 79 (12.70 μm) .

Surface Temperature, TS, is calculated according to Split window algorithm (Sobrino et al., 1997, 1998) for *AVHRR*:

$TS=T4+1.40(T4-T5)+0.32((T4-T5)^2)+0.83+(57-5W)*(1-\varepsilon)-(161-30W)D\varepsilon$ Eq (7.18)

where

T4 and T5 are thermal bands 4 (10,3-11,3 μm) and 5 (11.5,-12,5 μm);
W is water vapour content (1,7 gr/m²) measured at overpass time,
ε is surface total emissivity, calculated as the sum of three cases showed above and
D ε is the emissivity difference from threshold method, as follows:

$D\varepsilon = -0.003-0.029b1$

where b1 is AVHRR band 1 (0.58-0.68 μm)

for *NDVI<0.2*

$D\varepsilon = 0.006*(1-PV)$ Eq (7.19)

where PV is vegetation cover (Eq 6.13)

for $0,2 \leq NDVI \leq 0,5$ and

DE=0 for NDVI> 0.5

ASTER: Temperature corresponds to kinetic temperature band, Band 12 (9.075 μm) and

AHS bands used correspond to thermal channels 71 (8.46 μm) to 80 (12.50 μm)

The incoming shortwave and long wave radiations were measured on ground by the meteorological stations (Common data index, Cdi in figure 8)

Seguin and Itier, 1983, statistically developed a relationship between instantaneous and daily net radiation flux (Eq 7.20) as:

$$Rnd / Rni = 0.30 \pm 0.03 \qquad \text{Eq (7.20)}$$

$$G = Rn\ 0.5\exp(-2.13MSAVI) \qquad \text{Eq (7.21)}$$

where:

MSAVI is a vegetation index proposed by Qi et al , 1994 (see Eq 3.40)

Evaporative fraction, **Λ,** is the ratio of evaporation (LET) over available energy (Rn –G). Roerink proposed a new definition for the evaporative fraction derived graphically from representing albedo, α, vs. surface temperature, Ts. To apply present model, we must remember that the image must include water saturated (wet), like water bodies and irrigated land, and dry areas like bareland or fallow land during summer. For low albedos, surface temperature is almost constant, which means all energy is used in the evaporative process (latent heat, T_{LE}) and just a little energy is consumed to increase temperature (sensible heat, T_H). Then, temperature increases along with albedo and as albedo increases, less water is available and more energy is used to raise temperature, this is known as "evaporation controlled". Finally, after some value, for high albedos, temperature starts decreasing, this means there is no available water for evaporation and all available energy is used for surface heating with a net radiation decreasing (cause more energy is reflected out of the system), this is known as "radiation controlled" (see graphs 7 to 9 and tables 17 to 19). When latent heat is maximum, sensible heat turns minimum (zero) and vice versa. For three sensors plotting of albedo vs. surface temperature was made and the output is a cloud of points with a general greater oscillation in temperature for low and medium albedo values and narrower as albedo increases. Both, radiation and evaporation controlled are represented graphically with two straight lines enclosing all plotted points. These lines and their associated equations represent extreme values for dry and wet conditions and simultaneously, with surface temperature- albedo plot, define the evaporative fraction as the ratio of the difference between radiation controlled and surface temperature-albedo over the difference between radiation controlled and evaporation controlled, as follows (Eq 7.22):

$$\Lambda = \frac{TH - TS}{TH - TLE} \qquad \text{Eq (7.22)}$$

Model performance depends on accuracy of different terms in the equation and since other measured variables in model are basically limited or defined by sensor type, accuracy for *Evaporative Fraction* also depends on number plotted dots, thus, with highest resolution sensor, more plotted dots (scan spots) can be used within the same image and consequently the oscillation for the *Evaporative Fraction* can be seen clearer.

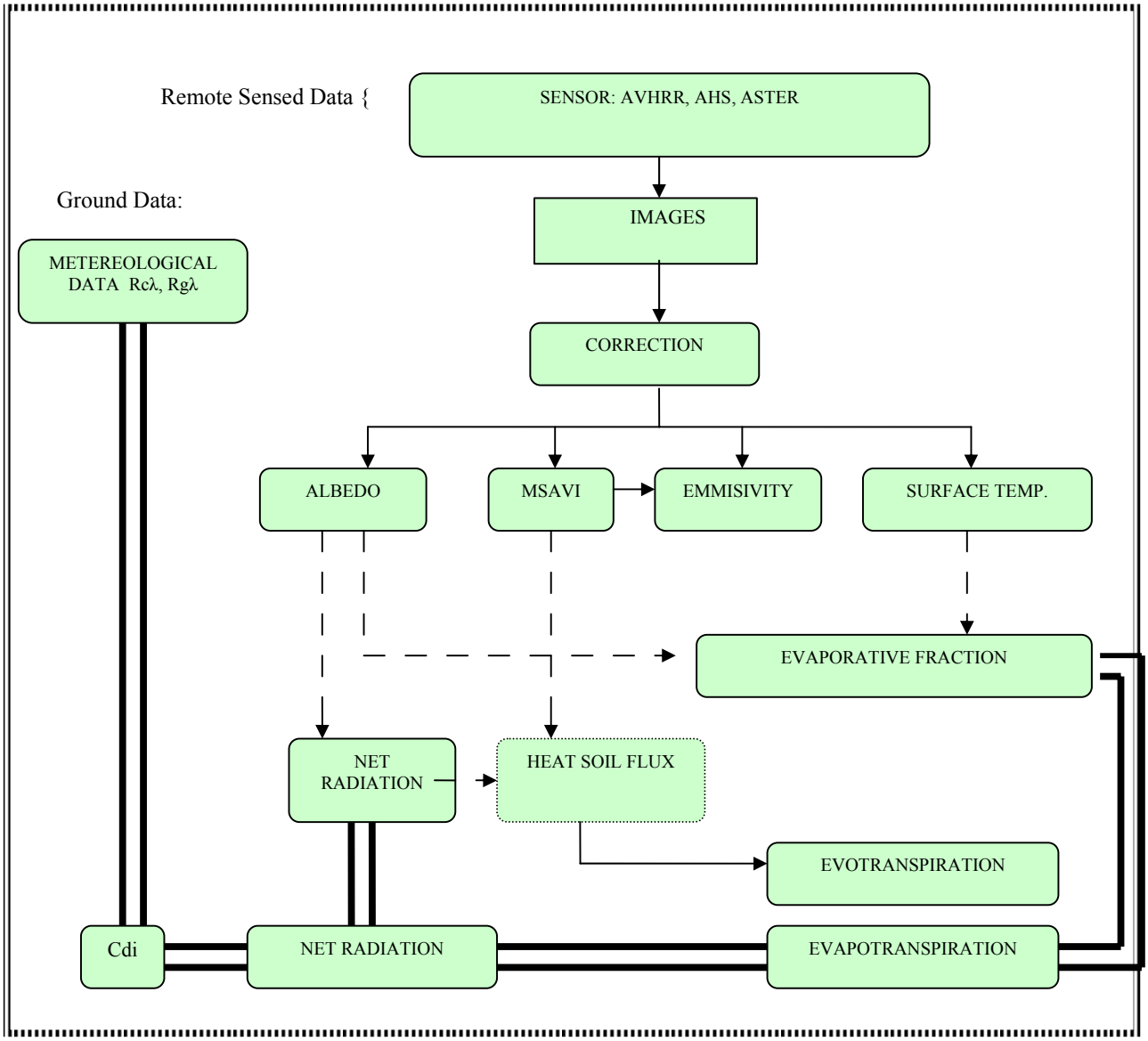

Figure 8 Flowchart for S-SEBI model application, adapted from Gómez et al., 2004.

8 RESULTS

The scope of present work is limited by number of ground measurements to corroborate model. Within the whole image for study area there are only lysimetric data -Las Tiesas- including two different crops (grass-*Festuca arudinacea*- and barley –*hordeum vulgare*- with the same crop coefficient) with ET measurements every 15 minutes during the test day. In general a weighing lysimeter is a device to evaluate soil water quantity with respect to time (Aboukhaled *et al,* 1982). It basically is a rectangular section containing soil, supporting the studied crop, lying on a scale that accounts for water losses (ET) or entries (irrigation, precipitation) in the system by a simple mass balance. First, data had to be screened because external interferences like accidental stepping by people or animals. The screening was a simple linear relationship between net radiation and ET within 15 minutes periods and some interference was only found in the grass lysimeter where, after adjusting, a value of 6,72 mm/day was calculated. A value of 4,18 mm/day was found for barley without any correction.

8.1 Model application

A characteristic of S-SEBI model is that it was conceived and first used to retrieve ET from remote sensed images and, though it is a physically based method using semi empirical relationships to derive an algorithm (numerical solution), its most suitable solution is through a digital image treatment. Because operational and computing requirements, *ENVI* ® and IDL® image analysis software was used. It allowed to visualize, correct and digitally operate with different algorithms involved in the model. As said before, images are created by amount of radiation scanned by sensor converted by a computer display into digital counts (values and their frequencies) conforming a matrix-like arrangement that afterwards can be used in calculations. Even though numerical values from images can be generated in text format files (e.g. txt extensions) useful to check and extract information, the best way to go all the way through different calculations retrieving ET is to operate between images directly. Different formulas can be solved by a basic tool called "*band math*". Next, applied procedure and results are commented.

8.2 Pre processing

After data acquisition (satellite and aircraft overpass) and before any operation is done among the images, surveyed data must be adjusted in order to get reliable results for any application. It was before mentioned that La Mancha province is a flat terrain with no significant variations in altitude (less than 2 m at the study site) which makes the area an appropriate place to validate models used in remote sensing. Nevertheless, we must remember that Earth surface is not uniform even if it appears so for the human eye. Due to nature of remote sensing techniques, data are acquired from a distant target (the

Earth), which has a non regular surface, and travel through a medium (atmosphere) with usual unsteady conditions. This means that some corrections have to be done before performing any use of them.

Image pre-processing include enhancement (statistical), visualization techniques, etc, but for detailed studies radiometric, geometric corrections and digital classification are usually applied. Images used in present work had a different digital treatment.

8.2.1 Geometric corrections

It is logical that sensor flight track during data acquisition is not exactly oriented with a referenced map system, thus, before any applied use of images a matching process of the image must be done in accordance with a known coordinate system. Besides that, some errors are caused by distortions, Earth rotation and curvature and platform oscillations (GCU). Procedure of correcting images is out of the scope of present work. Anyhow main corrections are described as follows:

Ground Control Points (GCP): this method allows matching two images, the one we want to correct (warp) and one that was already corrected (base image). Overlaying procedure is made through selection of a set of points, which number depends on the image complexity (topography features) and size. Control points must be uniformly spread all over the image. When both images are displayed, selection process is made through *Map* and *Registration* commands. Every GCP is first selected on the *base* image and then in the *warp* one, then after all points are gathered (*Add point* command) a final check is made before assigning definitive coordinates for the corrected image. Different bands from the same sensor may have different scales, that was the case for thermal bands in ASTER images (90m pixel), which had to be resized to be able to operate with the visible ones to retrieve parameters like albedo and emissivity. Images were geo referenced using the geographic coordinates and the UTM projection.

8.2.2 Atmospheric correction

One condition for the model to be applied is a cloud free weather during the study day. Images were almost completely cloud free at the test site but due to satellite and aircraft overpasses were not exactly done at the same time. Some low clouds spots were observed in the AHS images. Fortunately it did not cover up a significant area of the image and ground measured data site (lysimeter) were not affected in any of the images. ASTER and AVHRR images were cloud free. Even if this condition was met, still atmospheric gases mixture (O_3, CH_4, CO, N_2O, etc), aerosols and mainly water vapour that absorbs and scatters part of the radiation cause some perturbation (e.g. haze) present in images. To counteract the effect caused by atmosphere different computer codes based on the *radiation transfer equation* (chap. 3) are used.

Program PCMODWIN 4.0 (in FORTRAN language), an enhanced version of former programs as LOWTRAN 7 (Kneisys et al, 1.988), was applied to make atmospheric corrections in present work. It covers the electromagnetic spectrum from 0 to 50.000 cm^{-1} (0,2μm to ∞) and is based on High- Resolution Transmission HITRAN, a database containing spectroscopic parameters (Rothman et al, 1992). Absorption coefficients (self-boardening coefficients) that depend on water vapour concentration were reduced (around 20%), based on lab measurements made by Devir et al, 1987. Molecular scattering and aerosols processes are also considered (Rayleigh, Mie, multiple). The program calculates trajectory of radiance through atmosphere accounting refraction and curvature. It includes representative models of six standard atmospheres, including aerosols, clouds and rain which may be defined by user, thus pressure, temperature and humidity profiles, measured by radio sounding, can be input to the program. For present case, a mid latitude summer atmosphere was used. Evaluation of molecular transmissivity due to absorption, in solar and thermal spectra, is made the Voigt profile (Kalkins, 2002). For aerosols, atmosphere is divided in four regions (0 to 2 km, 2 to 10 km, 10 to 30 km and 30 to 100 km) considering variation in height, humidity and season. One of the new features of the used program, compared to former versions, is its *multiple dispersion model* (Isaacs,1987) that considers returning of part of the dispersed radiation. The output of PCMODWIN4.0 is the atmospheric radiance (ascending and descending) and transmissivity for considered atmosphere and observation angle. Finally data are screened and exported to Excel, (if needed) with radiance and transmissivity values that can be used to retrieve parameters used in model; surface temperature from 4 and 5 bands and albedo from bands 1 and 2 in AVHRR sensor. Similar procedure was applied to ASTER sensor using 1 to 3 and near infrared bands for later calculations of albedo and temperature respectively. In general the applied model for AHS sensor is the same, except that the radiative transfer code has a basic change due to flight height (1.000 m) comprising only a lower region of troposphere (known as boundary layer).

Other modules like the Simplified Method for Atmospheric Correction, SMAC (Rahman and Dediu, 1993) can also be used for the same purpose with some limitations. Solution and comprehensive support of atmospheric transference computing codes, which are out of the scope of present work, are found in Devir, A.D, The U.S. Air Force Geophysics Laboratory literature, Berk, A., Lenoble, J., among others.

8.3 Evapotranspiration estimation

Once images are corrected and geo referenced acquired data can be used to retrieve ETd in Barrax field (the aim of present work), so:

As explained in former chapter, latent heat is the amount of energy used in the ET process. To estimate it, *Evaporative Fraction*, Λ (Eq.7.22), and energy balance fluxes (*Rn, G*) have to be retrieved from images. From equation 7.2 we see to compute net radiation flux, Rn, albedo, α, emissivity, ε, and surface temperature, *T*, have to be calculated. To compute emissivity, the Normalized Vegetation Index *NDVI* (Eq. 3.39)

has to be first estimated and for temperature, the S*plit Window* algorithm is applied (Eq 7.18). Another vegetation index, the Modified Soil and Vegetation Index, *MSAVI*, has to be used as well to compute the Geothermal flux, *G*. Short and long wave incoming radiation, also used to compute net radiation flux, were ground measured by common hand radiometer at the meteorological station.

Continued, results for every term in Equation 7.1 are compared for different sensors and daily ET value is contrasted with ground based measurements and Jackson model to find applicability and relationships between sensors. For practical purposes, values for different variables and sensors are computed in ten different points, pixel based and areas (tables 13 to 16) including the lysimetric measurement (S). All computes are made through images using Envi + IDL ® program including Jackson model which is a linear relationship between Rn (in mm) and ET (mm) and can be used to extrapolate ET values from images based on meteorological measurements.

Table 13. Noaa, Aster and AHS ETd results and terms used for its retrieval at Barrax field on 17 08 04

Coordinate (N: W)	*ETd (mm/d)*			*Rn W/m²*			*G W/m²*			*Λ*		
	3.63 (lys barley)			173.7(S. lys barley)								
POINTS	Noaa	Aster	AHS	Noaa	Aster	AHS	Noaa	Aster	AHS	Noaa	Aster	AHS
S: 39.059N 2.097W	2.96	2.84	2.70	169.48	170.4	151.8	19.97	33.12	20.72	0.56	0.50	0.62
P1: 39.064N 2.091W	1.33	6.63	5.38	149.10	226.63	179.07	22.00	28.12	9.74	0.30	0.94	0.90
P2: 39.068N 2.112W	1.33	2.45	1.94	149.81	185.65	114.78	21.35	32.56	16.13	0.30	0.45	0.56
P3: 39.072N 2.126W	3.24	5.90	4.69	169.50	213.28	174.95	20.81	25.50	16.40	0.62	0.89	0.84
P4: 39.079N 2.092W	0.96	2.50	2.20	142.98	187.58	130.60	21.08	32.14	19.27	0.22	0.45	0.56
P5: 39.057N 2.122W	3.55	6.25	5.90	171.66	221.07	219.19	18.42	25.76	25.43	0.65	0.90	0.86
P6: 39.067N 2.116W	3.20	1.15	1.74	169.50	174.38	115.69	20.81	30.94	16.88	0.62	0.22	0.50
P7: 39.063N 2.086W	1.34	2.60	2.38	149.10	192.89	141.33	22.00	32.86	20.63	0.30	0.46	0.56
P8: 39.070N 2.119W	3.24	4.01	3.51	169.50	202.26	153.82	20.81	34.58	18.28	0.62	0.67	0.73
P9: 39.074N 2.092W	0.96	2.20	1.41	142.98	184.20	112.42	21.08	32.58	16.90	0.22	0.41	0.42
P10: 39.068N 2.130W	3.24	6.90	5.40	169.50	222.96	173.55	20.81	25.39	9.60	0.62	0.99	0.93
Areas (km²)	Noaa	Aster	AHS	Noaa	Aster	AHS	Noaa	Aster	AHS	Noaa	Aster	AHS
A1: 0.4212 39.064:2.093	1.33	6.30	5.29	149.10	223.44	180.17	22.00	28.51	10.97	0.30	0.91	0.88
A2: 0.6480 39.054:2.106	3.14	6.00	5.19	167.76	222.20	184.68	20.22	29.22	13.49	0.60	0.88	0.86
A3: 0.4212 39.062 : 2.107	3.14	2.38	2.05	167.76	186.68	125.33	20.22	31.40	16.21	0.60	0.43	0.53
A4: 0.3321 39.066:2.121	2.30	3.95	3.28	170.57	202.11	156.42	19.6	34.53	22.01	0.63	0.66	0.69

A5: 0.2106 39.072: 2.115	1.33	2.16	1.84	149.81	183.67	115.71	21.35	32.17	16.51	0.29	0.40	0.63
A6: 0.2754 39.061:2.099	1.60	2.82	2.54	152.83	191.35	136.04	20.60	31.72	17.28	0.36	0.49	0.59
Pixel (≈2.653 km²)	Noaa		AHS	Noaa	Aster	AHS	Noaa	Aster	AHS	Noaa	Aster	AHS
Px1:39.083N 2.133W	3.24	4.14	3.56	169.50	201.62	149.67	20.80	30.04	15.53	0.61	0.66	0.71
Px2:39.083N 2.116W	1.34	2.29	2.19	149.81	184.88	124.09	21.35	31.45	16.23	0.29	0.40	0.55
Px3:39.083N 2.099W	0.96	1.94	N.I	143.00	181.73	N.I	21.08	31.47	N.I	0.22	0.35	N.I.
Px4:39.083N 2.083W	0.12	1.50	N.I	131.64	178.02	N.I	20.66	31.04	N.I	0.04	0.28	N.I
Px5:39.099N 2.066W	0.70	3.05	N.I	141.56	193.01	N.I	20.80	30.69	N.I	0.16	0.50	N.I
Px6:39.083N 2.066W	0.96	1.88	N.I	145.84	181.80	N.I	21.49	30.91	N.I	0.22	0.33	N.I
Px7:39.083N 2.049W	2.41	2.28	N.I	164.60	185.83	N.I	21.23	31.04	N.I	0.47	0.40	N.I
Px8:39.099N 2.033W	0.28	3.91	N.I	135.94	201.68	N.I	21.17	30.09	N.I	0.07	0.61	N.I
Px9:39.083N 2.033W	3.03	2.60	N.I	170.75	189.58	N.I	20.04	31.28	N.I	0.57	0.44	N.I
Px10:39.066N 2.133W	3.55	4.23	4.03	171.66	210.50	173.30	18.42	30.72	20.49	0.65	0.67	0.72
Px11:39.066N 2.116W	3.14	3.90	3.27	167.66	200.73	147.15	20.22	30.07	15.01	0.60	0.62	0.66
Px12:39.066N 2.099W	1.36	4.23	3.74	149.10	204.47	153.48	22.00	29.89	14.19	0.30	0.66	0.73

Table 14 Results (point based) for variables used to calculate terms in S-SEBImodel. Underlined values correspond to measured values at the Lysimetric Station.

Coordinate	*T(K)*			*Albedo* α			ε			*Vegetation Indices*				
	301	301	301	0.22	0.22	0.22				*NDVI MSAVI*				
	Noaa	Aster	AHS	Noaa	Aster	AHS	Noaa	Aster	AHS	Noaa		Aster		Ahs
L 39.059N 2.097W	316	305	317	0.20	0.11	0.28	0.97	0.96	0.95	0.3	0.6	0.0	0.5	0.5
P1: 39.064N 2.091W	321	300	302	0.20	0.07	0.23	0.97	0.99	0.96	0.1	0.6	0.5	0.6	1.0
P2: 39.068N 2.112W	322	316	322	0.19	0.11	0.33	0.97	0.96	0.95	0.2	0.6	-0.02	0.5	0.6
P3: 39.072N 2.126W	314	304	305	0.18	0.09	0.22	0.97	0.99	0.97	0.3	0.7	0.4	0.7	0.8
P4: 39.079N 2.092W	323	316	322	0.20	0.10	0.27	0.97	0.96	0.92	0.1	0.6	0.0	0.5	0.6
P5: 39.057N 2.122W	313	302	301	0.18	0.08	0.09	0.98	0.99	0.96	0.4	0.7	0.6	0.7	0.7
P6: 39.067N	314	321	325	0.18	0.12	0.29	0.97	0.96	0.96	0.3	0.6	-0.	0.5	0.6

2.116W												03		
P7: 39.063N 2.086W	321	316	323	0.20	0.08	0.22	0.97	0.96	0.94	0.1	0.6	0.1	0.5	0.6
P8: 39.070N 2.119W	314	310	312	0.18	0.09	0.26	0.97	0.96	0.93	0.3	0.7	0.0	0.5	0.7
P9: 39.074N 2.092W	323	317	330	0.20	0.11	0.28	0.97	0.96	0.91	0.1	0.6	0. 03	0.5	0.6
P10: 39.068N 2.130W	314	300	300	0.18	0.08	0.26	0.97	0.99	0.96	0.3	0.7	0.6	0.7	1.0

Table 15 Results (area based) for variables used to calculate terms in S-SEBImodel.

Coordinates	*T(K)*			*Albedo* α			ε			*Vegetation Indices NDVI-MSAVI*				
Areas km²	Noaa	Aster	AHS	Noaa	Aster	AHS	Noaa	Aster	AHS	Noaa		Aster		Ahs
A1: 0.4212 39.064:2.093	322	301	302	0.20	0.07	0.23	0.97	0.99	0.95	0.1	0.6	0.5	0.6	0.9
A2: 0.6480 39.054:2.106	315	302	304	0.18	0.07	0.20	0.97	0.99	0.96	0.3	0.7	0.4	0.6	0.9
A3: 0.4212 39.062 : 2.107	315	316	324	0.18	0.10	0.28	0.97	0.96	0.93	0.3	0.7	0.0	0.5	0.6
A4: 0.3321 39.066:2.121	314	310	315	0.18	0.10	0.23	0.97	0.96	0.94	0.3	0.7	0.0	0.5	0.5
A5: 0.2106 39.072: 2.115	322	317	324	0.19	0.11	0.32	0.97	0.96	0.92	0.1	0.6	-0. 02	0.5	0.5
A6: 0.2754 39.061:2.099	320	315	320	0.19	0.10	0.26	0.97	0.96	0.94	0.2	0.6	0.1	0.5	0.6

Table 16 Results (pixel based) for variables used to calculate terms in S-SEBImodel

	T(K)			*Albedo,* α			ε			*Vegetation Indices NDVI-MSAVI*				
Pixel (≈2.653 km²)	Noaa	Aster	AHS	Noaa	Aster	AHS	Noaa	Aster	AHS	Noaa		Aster		Ahs
Px1:39.083N 2.133W	314	310	313	0.18	0.09	0.27	0.97	0.97	0.93	0.3	0.6	0.2	0.6	0.7
Px2:39.083N 2.116W	322	316	322	0.19	0.11	0.31	0.97	0.96	0.89	0.2	0.6	0.3	0.5	0.6
Px3:39.083N 2.099W	324	318	N.I.	0.20	0.11	N.I	0.97	0.96	N.I.	0.1	0.6	0.0	0.5	N.I
Px4:39.083N 2.083W	328	320	N.I.	0.21	0.11	N.I	0.97	0.96	N.I	0.1	0.5	0.0	0.5	N.I
Px5:39.099N 2.066W	325	314	N.I.	0.20	0.10	N.I	0.97	0.97	N.I	0.1	0.6	0.1	0.5	N.I
Px6:39.083N 2.066W	324	318	N.I.	0.19	0.11	N.I	0.97	0.96	N.I	0.1	0.6	0.0	0.5	N.I
Px7:39.083N 2.049W	318	317	N.I.	0.17	0.10	N.I	0.97	0.96	N.I	0.2	0.6	0.0	0.5	N.I
Px8:39.099N 2.033W	327	311	N.I.	0.20	0.09	N.I	0.97	0.97	N.I	0.1	0.5	0.2	0.6	N.I
Px9:39.083N	315	316	N.I.	0.17	0.10	N.I	0.97	0.97	N.I	0.3	0.7	0.1	0.5	N.I

2.033W														
Px10:39.066N 2.133W	313	309	312	0.18	0.09	0.19	0.98	0.97	0.94	0.4	0.7	0.2	0.6	0.7
Px11:39.066N 2.116W	315	311	316	0.18	0.09	0.25	0.97	0.97	0.94	0.3	0.7	0.2	0.6	0.7
Px12:39.066N 2.099W	322	309	312	0.20	0.09	0.26	0.97	0.99	0.96	0.1	0.6	0.3	0.6	0.8

Pixel Areas: Noaa 2653302.89 m² (1433,9 x 1850.41)
Aster: 8099.9 m ²
AHS:≈ 35. 9 m²

ETd value for the 18th of July 2004 was finally found for AHS, Aster, and AVHRR sensors at Barrax field. Chosen area to compare sensors performance comprise 20,26 Km² where only a lysimetric station (Las Tiesas, L) is available to contrast results. Net radiation, albedo and temperature measurements are also available in the station at overpass time. Since field data are only available in a single site in the whole considered area and data acquisition by sensors is done instantaneously (just one overpass for each sensor), validity of obtained numbers by the model application for different sensors is difficult to attain.

Figures 9 to 12 and graphs 2 and 3 present results daily ET for used sensors. Eleven points, P, (including the lysimetric station), six areas, A, and twelve NOAA pixels, Px, (only five are included in the AHS image) with an approximate area of 2,653 Km² are chosen for comparison. A Noaa pixel contains approximately 328 Aster and 73703 AHS pixels.

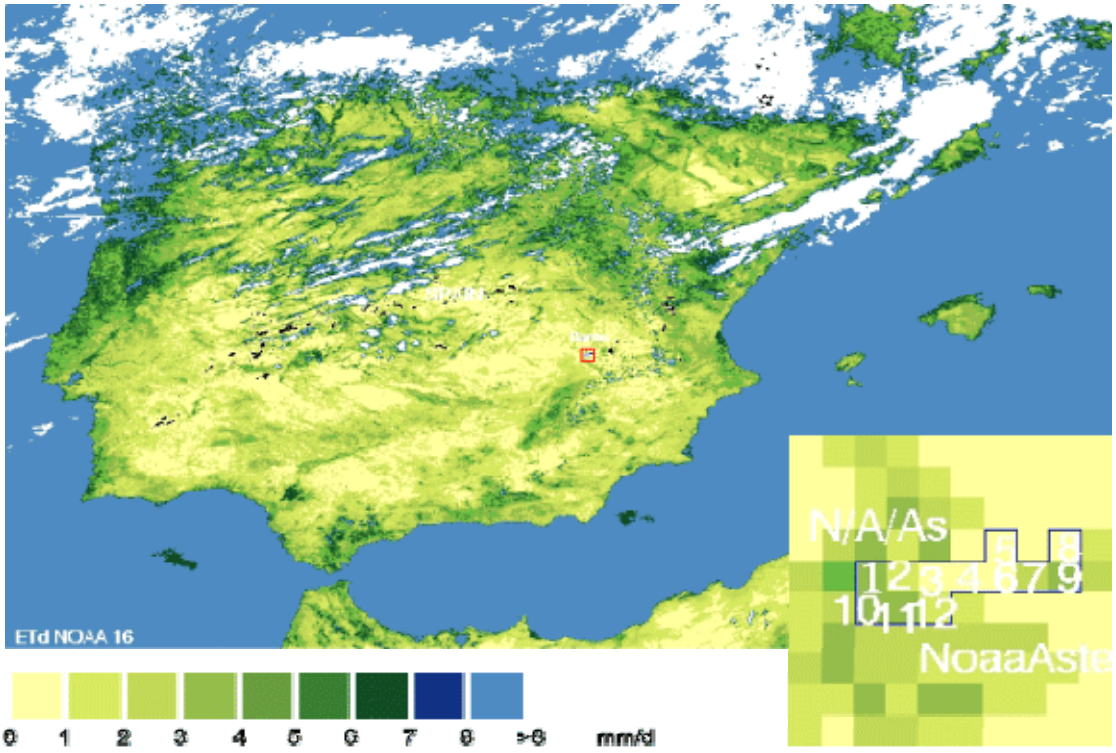

Figure 9. Daily Evapotranspiration at Barrax field (18-07-04). SSEBI model application using NOAA images.

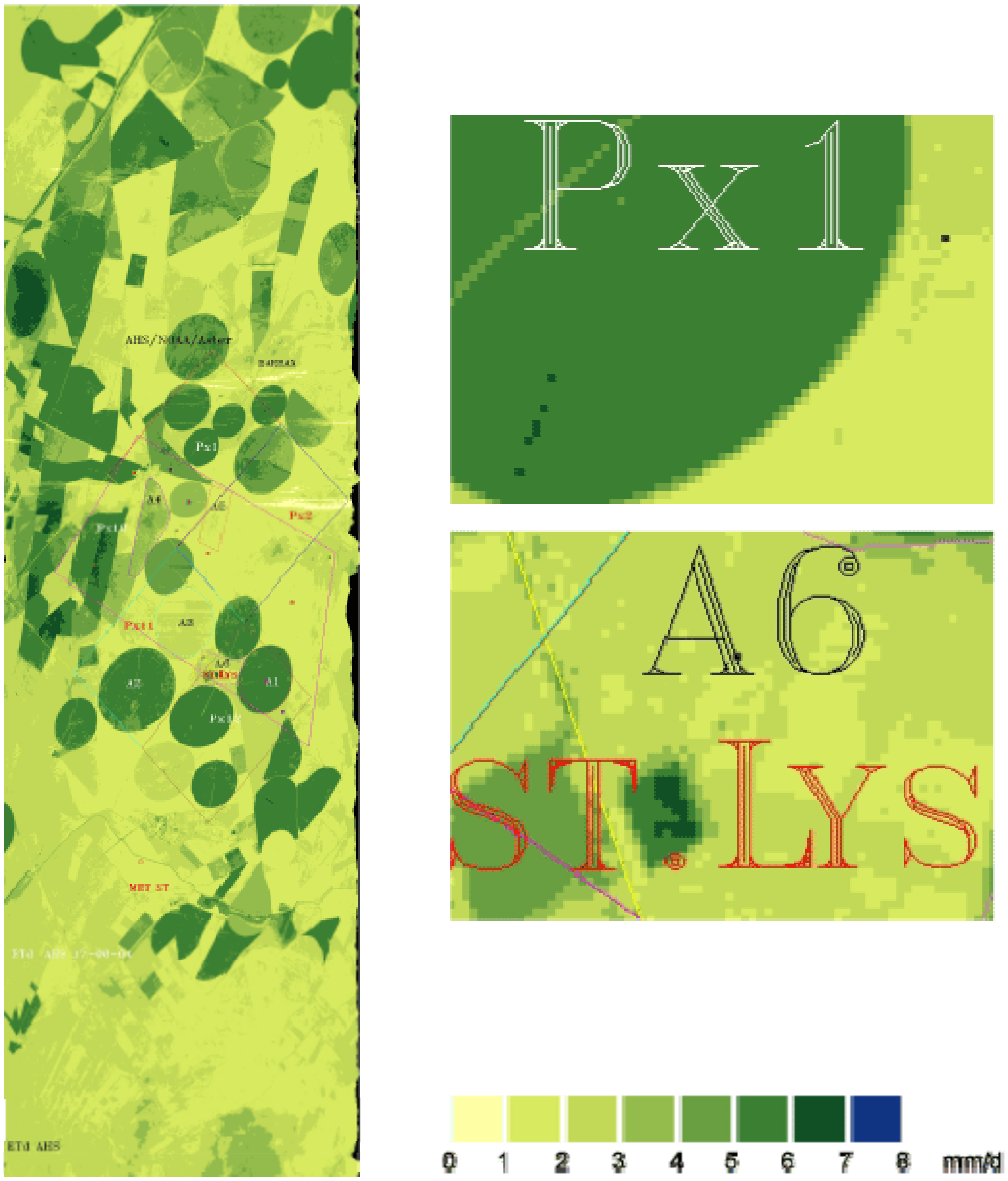

Figure 10. Daily Evapotranspiration at Barrax field (18-07-04). SSEBI model application using AHS images.

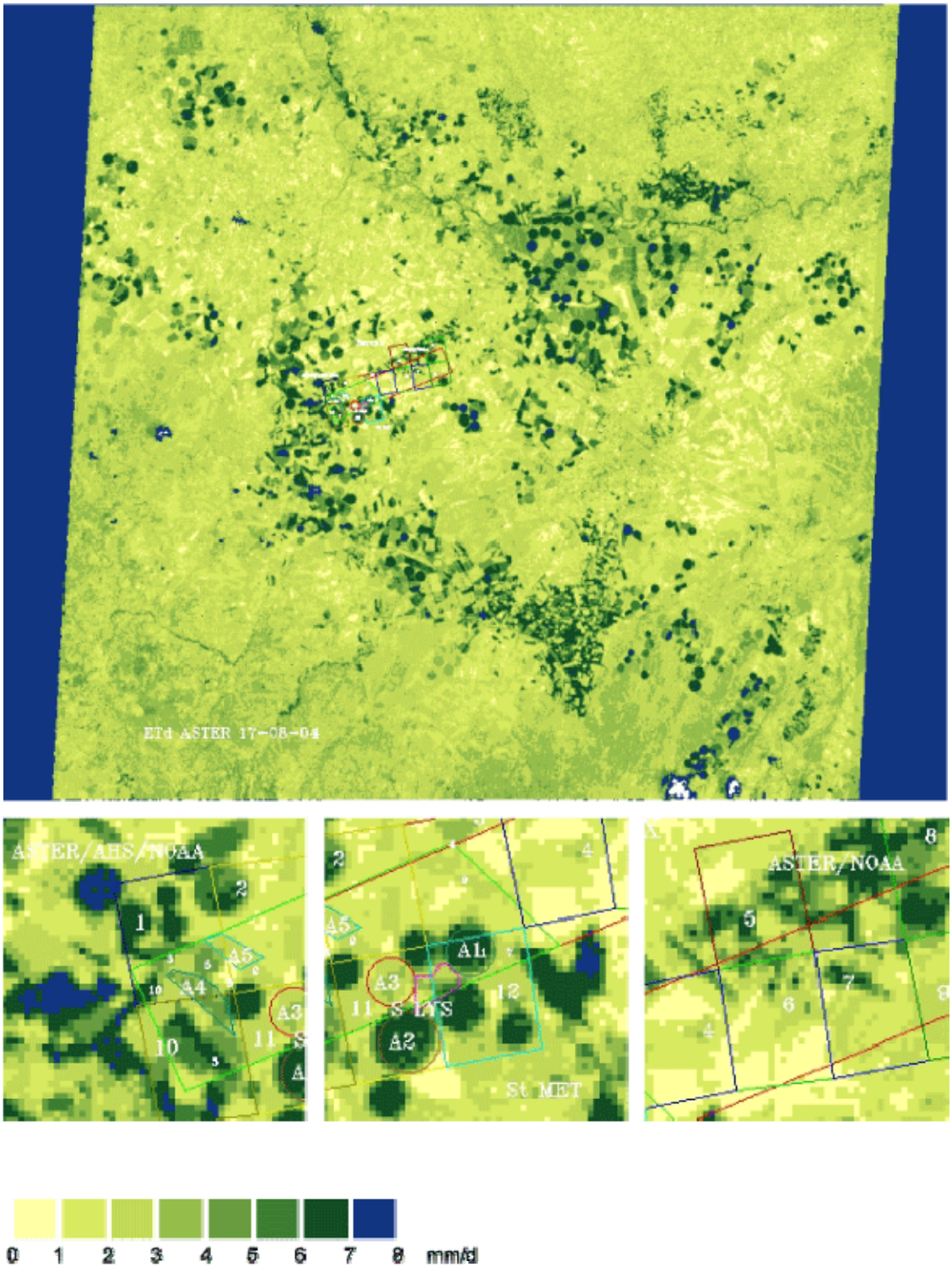

Figure 11. Daily Evapotranspiration at Barrax field (18-07-04). SSEBI model application using ASTER images.

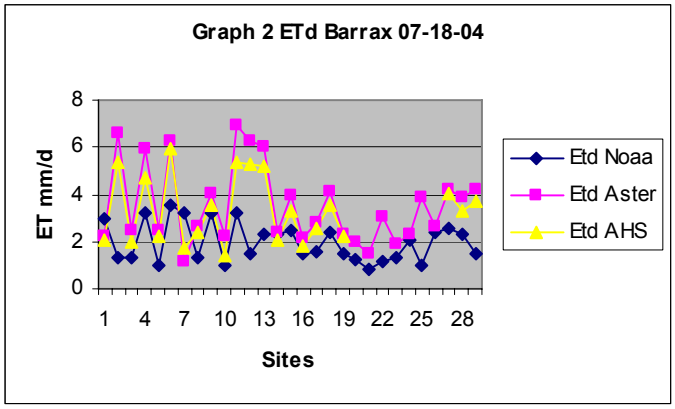

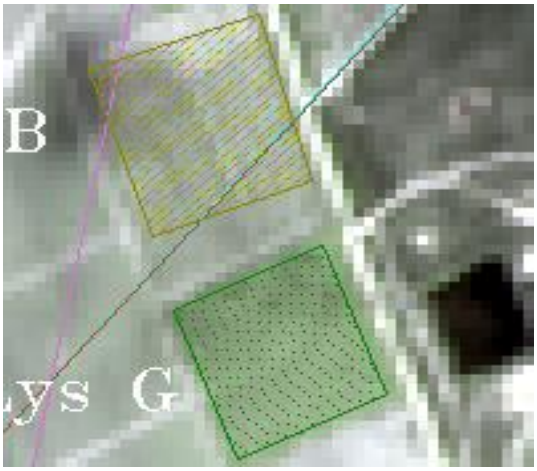

Fig 12: Lysimeters: Grass (G) and Barley (B)

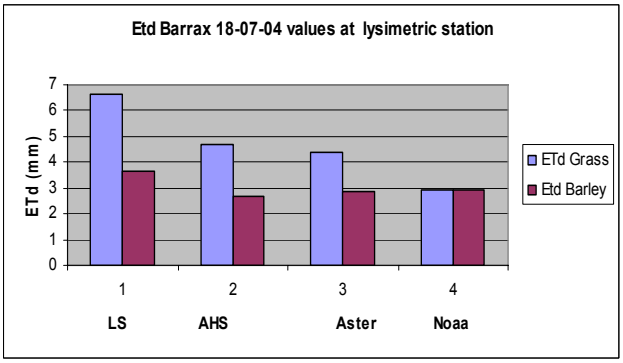

Graph 3. ETd mesured at lysimetric station and retrieved from different sensors.

Despite of fact of lack of enough measurements to validate and due to model and variables retrieval were applied and validated in other places and other sensors in the same place (*Sobrino* et al., 2003. *Jimenez* 2005), present study is focussed in comparing performance among the three mentioned sensors. Nevertheless, field data are use as reference for variables in model (ETd, T, α and Rn). Two areas were chosen to compare model output by the three sensors. An area of 8,132 km² is common for all sensors and a larger area of 12,126 km² is just covering available images for NOAAAs AVHRR and TERRA´s Aster. Sensors performance is evaluated for single points (AHS pixel based), specific sites with the same land use (less than 1 km²) up to areas covered by single Noaa pixels (2,65 Km²). For point based valuation 36m², 8100m² and 2.65km² areas, which correspond to pixel size for each sensor, are compared. Results for different terms in model (Λ, Rn, G) and variables used to compute these terms (α, T, ε, vegetation indices) are shown in tables 5.1 to 5.5. In most of cases, found values for ETd are higher for ASTER sensor (except P6 and A3 Px and Px9). ETd values showed a high correlation between AHS and Aster (0.96) and none of them did with Noaa (less than 0.3). Terms

involved in model show variations within different sensors output with a determinant weight of net radiation compute for ETd calculation in Aster cases while Evaporative fraction was the main factor when Noaa showed higher values. Variation and impact of different variables is next presented:

8.3.1 Net Radiation, Rn and the (Rn –G) term

Results of sensors showed underestimations of net radiation for Noaa (4%) and AHS (25%) and a difference of 6% over the value at the meteorological station (S). ASTER sensor account for the highest values in Rn and (Rn –G) term in all sites (see graph 4), except one point for the difference between Rnd and G (P 6 in graph 4) which showed higher value for Noaa. At this specific point it was probably due to the impact of high value of MSAVI index and consequent low value of G in the Noaa image at this point (the Noaa pixel covered not only cultivated land but also bare ground and fallow land which means more energy diverted down the ground) . When comparing Noaa and AHS values for Rn and (Rnd-G) term, the main tendency is higher values for Noaa except for 4 points (L, P1 in Px12, P3 in Px 1 and P5 in Px 10) 3 areas (A1in Px 12 and A2, A3 in Px 11) for Rnd and 5 points (L, P1, P2, P4, P10) and two areas (A1, A2) for (Rnd-G) term, probably also due to the influence of higher MSAVI indices in the AHS image at these sites. If we observe Eq 7.2, which retrieves Rnd in the model, its solution depends on field measured data (incoming short, $R_{c\lambda\downarrow,,}$ and long wave radiation, $R_{g\lambda\downarrow}$), which are the same for all sensors and cancel any possible interference with results, and model retrieved parameters emissivity, ε, *albedo,* α, and temperature, T. Out of these three parameters, emissivity show the least variation (around 0.03) between three sensors: values higher than 0.92 in all cases (except Px 4) for AHS, with measurements made directly by the sensor through a linear combination of channels 75 to 79, and values higher than 0.96 for Noaa and Aster, which retrieval was performed using the NDVI threshold semi-empirical method (Eq 7.3 to 7.17).

A variation of 0.01 in the emissivity value would mean a change of 3. 8 W/m² for all sensors in the term affecting incoming shortwave radiation and 4 ± 0.6 W/m² in the negative term of the equation. Temperature showed the highest values (330 K) for AHS followed by Noaa, with high values but small oscillations, and Aster. Oscillations also showed the highest value for AHS (33 K) while Aster showed 23K and Noaa 15K. Variations in temperature of 1 K mean changes around 6 W/m² for all sensors. When comparing temperature data with the meteorological station AHS showed a difference of 0,09% (3 K) while 2,7% (9K) and 3% (10K) were found for Aster and Noaa respectively. The remaining parameter involved in the Rn calculation is the *albedo,* α, which shows lower values for Aster*, fact that surely affected the portion of the incoming short wave radiation yielding higher values for the total net radiation in all cases*. Comparing other two sensors, AHS showed the highest values, except in two points, and the highest oscillations (0,24) while all Noaa values oscilated between 0.17 and 0.21. Aster also showed low oscillation in values. Finally it can be mentioned that the most decisive found factor affecting the Rn calculation was the albedo, since low Aster albedo

values implied high Rn values in all cases, except one case for AHS sensor which was also affected by a low albedo value. The physical meaning of low albedo values is that a smaller portion of the short and long wave incoming radiation is reflected back to the system (air-atmosphere) and a high portion of this energy remains available at surface. There were other two factors influencing Rn results: one was incoming shortwave radiation was less half of the total incoming radiation (around 41 %) for all sensors, making emissivity less important factor, and the other was temperature differences between sensors were not determinant enough to influence the total Rn value. In any case net radiation and the term (Rn-G), which represents the available energy in the system, were the most determinant factors in ETd calculation.

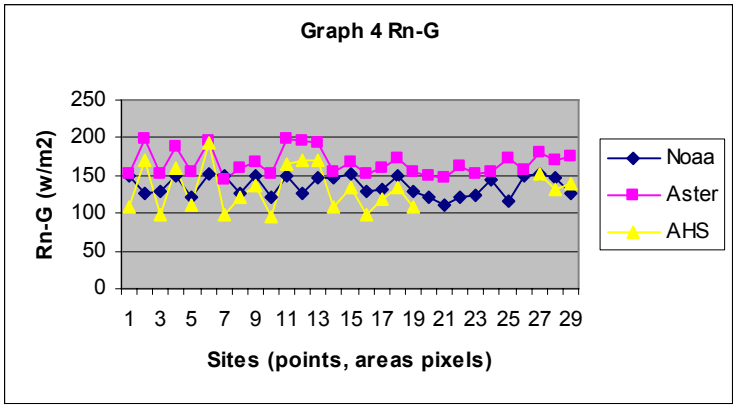

8.3.2 Evaporative fraction, Λ

Highest absolute values were found for Aster sensor but in most of cases AHS showed higher values than other two sensors (see *table 13*). There were only four cases where Noaa showed higher ETd values (P6, A3, Px 7, Px 9) and it was due to the impact of high evaporative fraction values. Temperature - Albedo plots were used to obtain the evaporative fraction and since these plots are pixel based more points were used according to sensor resolution. Thus AHS used 218575, Aster 3505 and 440 for Noaa. It should be mentioned that in the first two cases, the number of used pixels correspond to the studied area but in Noaa images, studied site only comprises 12 pixels which are not considered enough to see pixel oscillations of temperature with the same albedo values (440 were used). This range is related to water saturation degree (from dry to wet conditions).

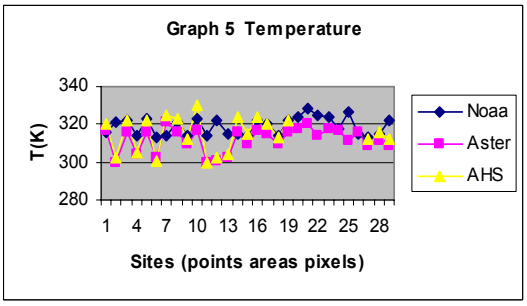

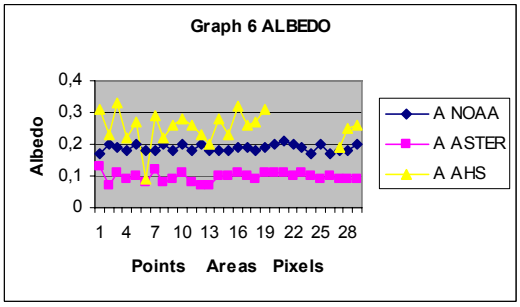

If the term (Rn –G) computes the available energy in the system, the evaporative fraction stands for fraction of this energy used in the ET process. In equation 6.22 it is seen that the evaporative fraction value depends on the ratio between the used and the available energy. As said before, AHS values were found to be higher in average affecting the ETd values but not with the same impact as net radiation, Rn (see table 13). The higher average of evaporative fraction seemed to be related, not exclusively, to the number of plotted pixels since probability of occurrence of lower temperature values for the same albedo is higher. High Λ normally happened in plot of lowest temperature values for different albedos, i.e. the closer values to the latent heat line (TLE) in graphs 7 to 9, the higher the ratio computing Λ; e.g. one point (P3) showed the fourth highest evapotrative fraction value for single points in all sensors with values of 0.84 for AHS (TH=364, TLE= 294, T= 305, α=0.22), 0.62 for Noaa (TH=329, TLE= 305, T= 314, α=0.18) and 0.89 for Aster (TH=329.5, TLE= 300, T= 304, α=0.09).

When lower albedo values start increasing, temperature is almost constant (evaporation controlled), i.e. all available energy is used in the evaporpotranspiration process (maximum latent and null sensible heat), thereafter some increase in albedo value, the temperature starts rising because part of the energy is used in the evaporative process and the remaining is consumed to rise the temperature (increase in sensible heat). This is due to change in moisture conditions for the evapotranspiration process until no water is available for it and all the energy is used to heat up the system. Finally after albedo values continue to increase, more energy is reflected back to the atmosphere with a drop in temperature since less energy remains available in the system and all the evaporable water has gone (radiation controlled). For instance, Aster Albedo values in all the studied sites oscillated between 0.07 and 0.16 while temperature fluctuated between 299 and 328 K. For some of the lowest albedo values, starting at 0.07, temperature plots did not grow (with constant 300 K) before certain value (0.085) where it started to increase with a high gradient until a albedo value around 0.143 (T=322) where started dropping for higher albedos (radiation controlled). This general behaviour of the albedo-temperature relationship was verified for every sensor with some differences shown above in tables and graphs below (:

Table 17. Evaporative Fraction, Λ, and o*scillations of albedo-temperature values at Barrax field on 18-07- 04 for AHS sensor at flight time*

Sensor	AHS						
α	min	max	mean	SD	EC		RC
	0.095	0.556	0.316	0.07	LV	UV	>
					0.10	0.26	0.33
T (K)	294.83	356.94	318.12	9.6	≈ 299,3		329.0
Equation	Λ=(-79,3α+377.1-T)/ (-112.87α-89.45)				TLE=33.5α+287.65		TH=-79,3α+377.1

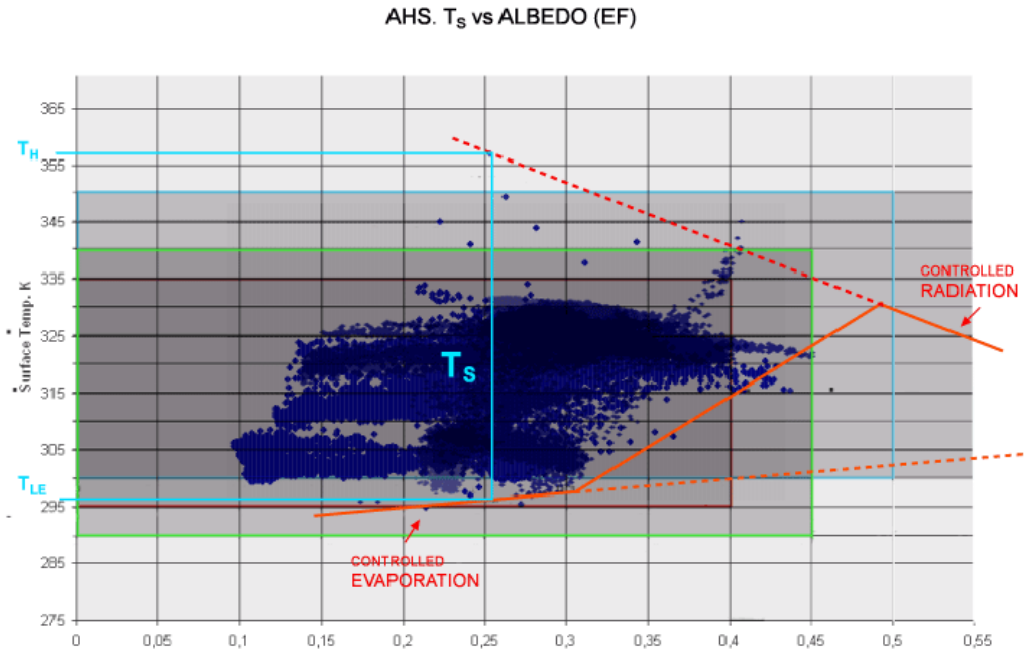

Graph 7. Evaporative Fraction, EF. Temperature- Albedo plotting area for AHS sensor at Barrax field 17-08-04

Table 18. Evaporative Fraction, Λ, and o*scillations of albedo-temperature values at Barrax field on 18-07- 04 for ASTER sensor at overpass time*

Sensor	ASTER						
α	min	max	mean	SD	EC		RC
	0.048	0.157	0.103	0.01	LL	UL	>
					0.07	0.048	0.13
T (K)	299.0	327.8	314.9	6.42	≈300		323
Equation	Λ=(-119.22α+339-T)/ (-245.23α+50.67)				TLE=126.01 α+289.22		TH= -119.22α+339

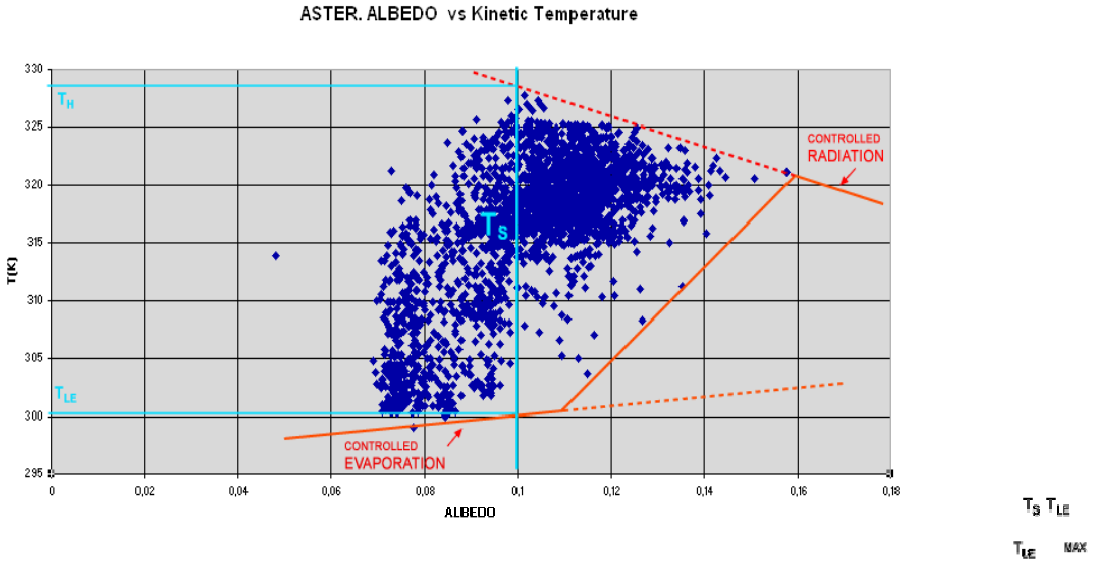

Graph 8. Evaporative Fraction, EF. Temperature- Albedo plotting area for ASTER sensor at Barrax field 17-08-04

Table 19. Evaporative Fraction, Λ, and o*scillations of albedo-temperature values at Barrax field on 18-07- 04 for AVHRR sensor at overpass time*

Sensor	AVHRR (NOAA)						
α	min	max	mean	SD	EC		RC
	0.111	0.325	0.190	0.02	LL	UP	>
					0.13	0.17	0.17
T (K)	303.5	329.4	322.18	4.70	303		327.6
Equation	Λ=(-22.459α+333.54)-T)/(-40.379α+31.64)				TLE=17,92α + 301,9		TH=-22,459α + 333,54

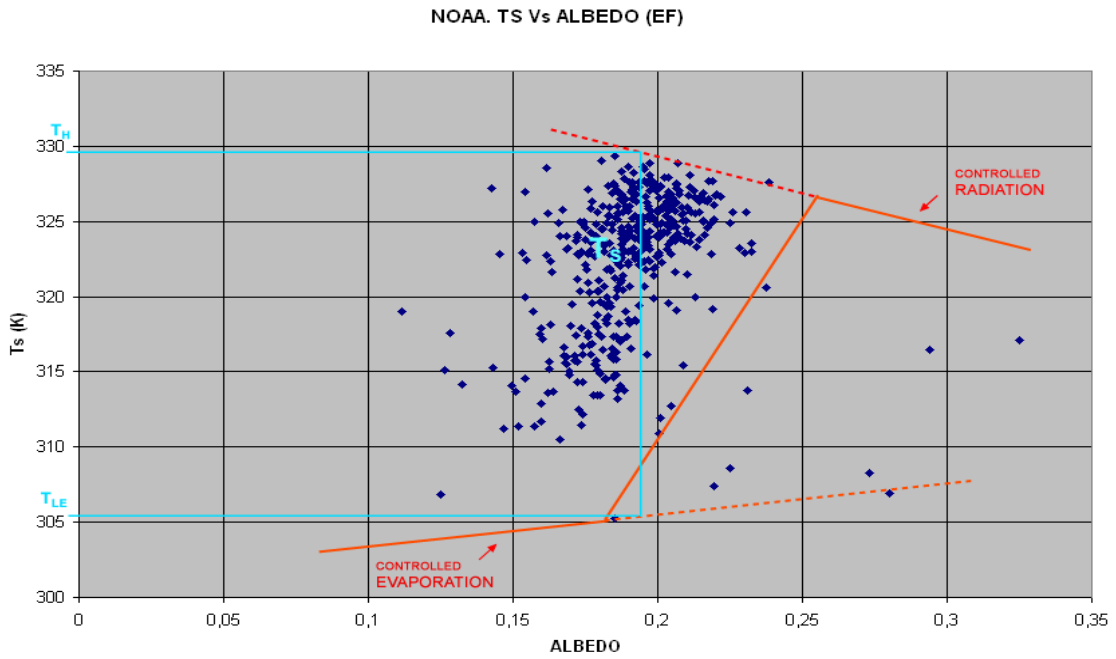

Graph 9. Evaporative Fraction, EF. Temperature- Albedo plotting area for Noaa´s AVHRR sensor at Barrax field 17-08-04

If we observe tables 17 to 19 and graphs 7 to 9, temperature values for the lower limit of controlled evaporation have similar values for three sensors (299 to 303 K) while albedo ranges do not. Analogous behaviour is shown for relationship between three sensors when temperature values start to decrease along with albedo increasing (radiation controlled). The continuous line indicate the albedo-temperature tendency. Values in between Controlled Evaporation and Controlled Radiation stand for different degrees of water saturation in observed pixels. A summary in graph 10 below shows the difference between model variables at barley lysimetric station and calculated for each sensor:

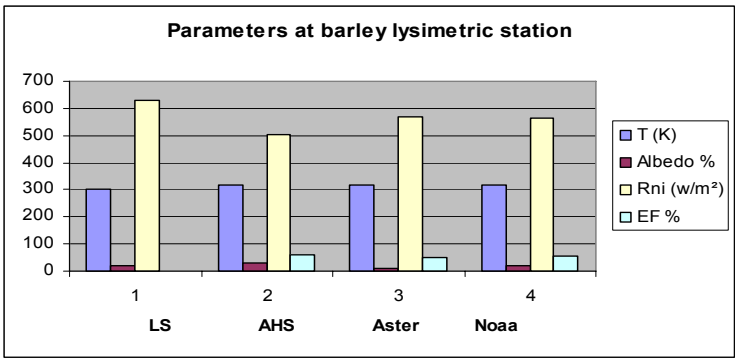

Graph 10.Parameters measured at the barley lysimeter (LS) and model retrieved

8.3.4 Vegetation Indices and Emissivity

The number of bands and type of wavelengths (windows) used to compute ET depend on sensor features but basically they use the same region. Bands used to compute ET in present work comprise observations channels in the visible and part the near infrared (thermal) for every sensor. In NDVI case (calculated for NOAA and Aster), Noaa values were, in general, lesser (tables 14 to 16) due to pixels comprised not only cultivated land but also fallow land and bare soil fields during the summer season. At the overpass time, irrigated crops had some degree of saturation since normally irrigation practices are done during the fist hours in the morning. In case of MSAVI (used in G flux for three cases) tendency was higher for AHS values and similar values for other two sensors affecting slightly the portion of available energy in the net radiation term. Despite of that, its influence was higher for not cultivated land or scarce vegetation pixels since it meant less available energy for the ET process and more radiation diverted (absorbed, transmitted) down to the ground (Geothermal). Emissivity, despite its low impact in total calculation, confirmed differences between cultivated and fallow land (from the images) according to NDVI values. High MSAVI values also confirm contrast between irrigated and non irrigated land. Figures 13 to 18 show the three ranges of NDVI values for Aster and Noaa (white to grey values represent pixels within the range):

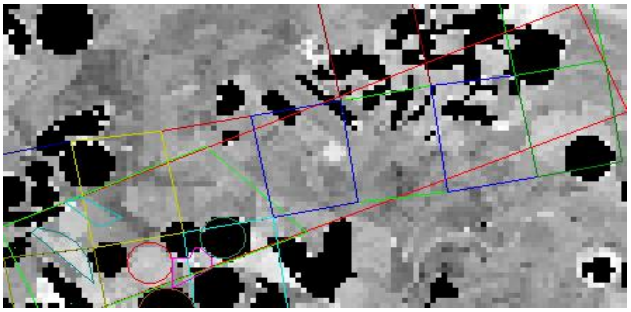

Figure 13. NDVI values less than 0.2 for ASTER image

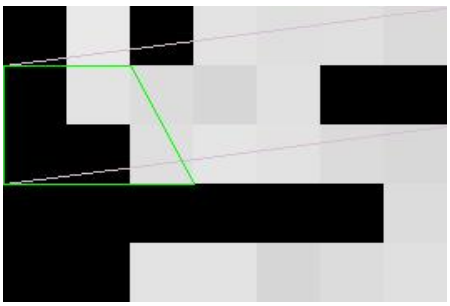

Figure 14. NDVI values less than 0.2 for Noaa image

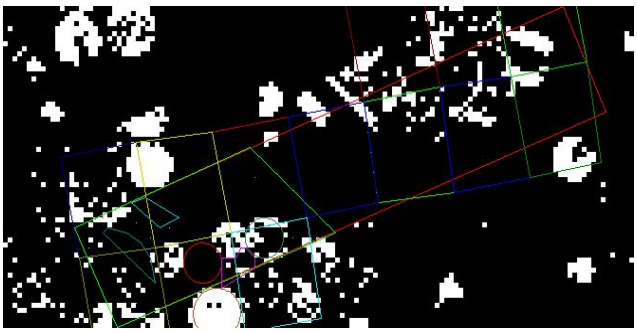

Figure 15. NDVI values from 0.2 to 0.5 ASTER image

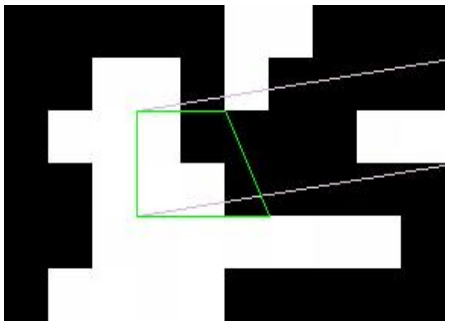

Figure 16. NDVI values from 0.2 to 0.5 Noaa image

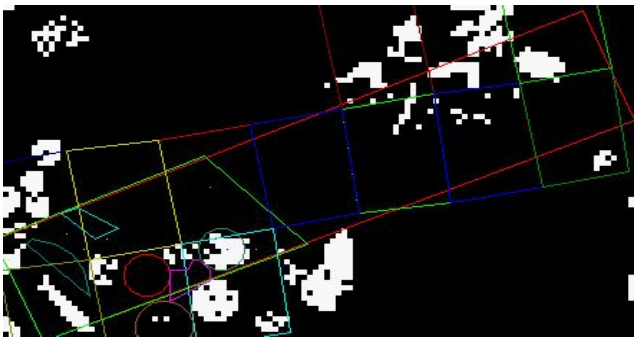

Figure 17. NDVI bigger than 0.5 ASTER image

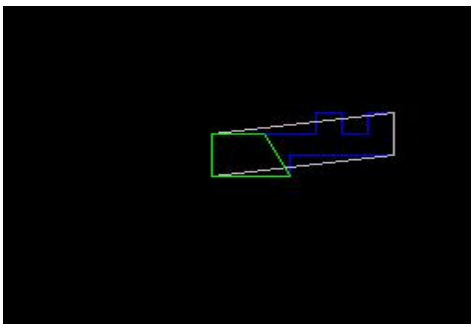

Figure 18. NDVI values bigger than 0.5 Noaa image

8.4 ET calculation using Jackson Model

This model has a similar approach to energy budget balance models but accounting for the aerodynamic resistances which are not consider as independent parameters in Roerink´s model (making the model much more operational). In this case, since no data are available about specific climatic and, mainly, crop parameters, its computation only make use of net radiation, Rn, and ET. The model assumes a linear relationship between available energy Rn, expressed in mm/day, and ET values for 15 minutes periods during the test day. Correlation coefficient, R, showed a value of 0,75 and a daily ET value of 6,78 mm/d at meteorological station in the grass lysimeter (6,72 mm/d was the actual). The equation resulting from the correlation between measured Rn and actual ET values at the lysimetric station are used for each sensor to compute ET.

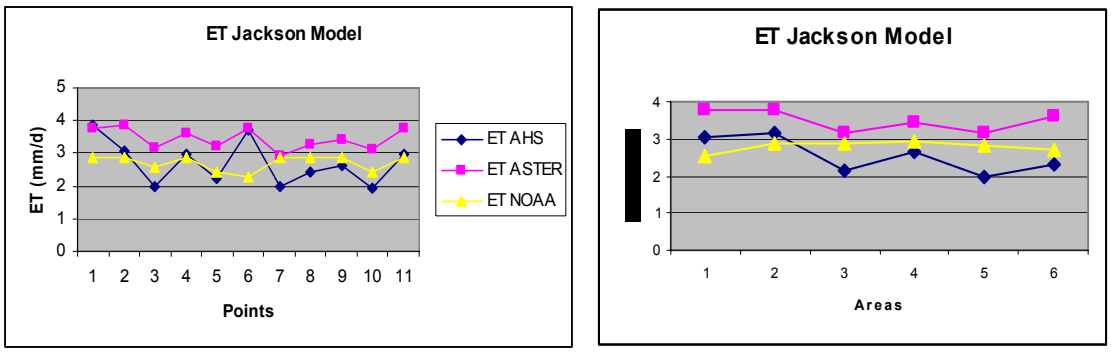

Graph 10 Daily ET (points, areas) using Jackson Model at Barrax field 17-08-04

Here, since ET is only dependant on net radiation, results were identical to as Rn values. The most notorious fact is the low oscillation between values. This could mean that approximately the same energy amount is available in all places with a lesser impact of surface type, except perhaps albedo. Its calculation also confirms the high correlation coefficient (R^2) between Aster and Noaa (0.80 for points and 0.75 for areas) while Noaa kept values lower than 0.10, fact that is remarked by the spatial resolution since the same value (in the same Noaa pixel) is used for points with evident different land use in the other two sensors image.

8.5 Conclusion

After SSEBI model use, it becomes obvious about its applicability on daily ET retrieval using remote sensed information (images). There is no doubt about its potential in natural and water resources management. It is remarkable the relative low information input, just a few visible and near infrared bands by the sensor and incoming radiation on the ground, to calculate the water loss for vegetated areas. Algorithms used in the model incorporate, both from empirical and conceptual models, different factors that have to be accounted explicitly in other models. As expressed by Di Bella et al., 2000, "topographic effects, water surfaces influence, wind, roughness, surface and atmospheric temperature differences and other important factors affecting ET measurements are in some way accounted in energy balance models". Most of other models, even ground based, demand either too many variables or are really limited in spatial scale (lysimeters, Bowen Ratio, etc). Nevertheless, validation is a key factor in order to use it for extended areas.

Some important parameters like emissivity are derived from calibrated measurements in labs (spectral libraries) and even if they are extended, minerals and soil types or surfaces are much more diverse on the field. Barrax field has been used for more than two decades, since EFEDA experiment (Bolle et al., 1991), to validate and develop semi-empirical models used in remote sensing techniques, which means a huge amount of secondary information that can be eventually used.

Anyway if the model is attempted to use elsewhere, validation campaigns must be performed, during different seasons and years, to be able to apply the model consistently. Among all terms in the model equation, Evaporative Fraction was found to be the most sensitive between sensors. Its determination is the key factor to apply and validate the model in other sites. Number of plots depend on spectral and spatial resolution and just a single dot could change the slope when choosing TH and TLE equations. Despite albedo – temperature relationship had the same general behaviour for all sensors (continuous line in graphs 7 to 9), the slopes and breaking points change between sensors considerably. The other point is the spatial resolution and accuracy. It is expected the higher the resolution the better the retrieved results. Actually it can not be said that accuracy is just depending on the resolution. Measurement protocols, image pre-processing, sensor specialization and calibration are also important to reach reliable results.

Correlation factors were found to be high between AHS and ASTER (>0.78) for all used variables. NOAA showed lower values for daily ET in the studied area. It is logical since pixel size included different surfaces with relative high albedo and low NDVI values. This means higher resolution sensor could be considered for agricultural applications (irrigation purposes) with a previous careful validation. It is possible that medium spatial resolution satellites (like TERRA) can be used to retrieve daily ET values with appropriate land or airborne (like AHS) calibration means. AVHRR or low resolution sensors validation is more difficult to attain for agricultural purposes. Perhaps for extended mono cultures or other applications that do not demand high accuracy as irrigation practices do. Large basins or regional water balances, in equatorial forests with lack of meteorological data for instance, could be some of this uses.

One factor that is supposed to be a limitation factor for the model application is the cloud-free condition. Irrigation scheduling is performed during the dry season so it does not imply a great constraint for the model to be applied. The dry to saturated condition pixel presence in the image is not hard to meet either. Normally agricultural lands include water bodies or irrigated land.

Another limitation of model application is the expensive operative costs due to high tech techniques engaged. Many high resolution satellites are orbiting the Earth constantly at different latitudes. Purposes are diverse and the information needed to apply the model is the same used to perform other applications. In this respect, this constrain is just a question of priorities and market demands and regulations. After application is clear that operability and potential of the model is easy to see as a head start in future projects.

Despite mentioned limitations is easy to see that technological solutions, like applied in this work, suit better a demanding future in water resources management. Continuous remote sensing techniques enhancement is constantly made and remote sense applications, like ET retrievals, will surely be more diverse, accurate and affordable in a close future.

9 REFERENCES

ASTER. ***http://edcdaac.usgs.gov/aster/asteroverview.asp***

Carleton, A. M Satellite Remote sensing in climatology. Belhaven Press, London 1991.

Caselles, V., Delegido, J.,Sobrino, J.A. and Hurtado, E. Evaluation of the maximum Evapotranspiration over La Mancha region, Spain, using NOAA AVHRR data. International Journal of Remote Sensing, 1992 vol 13 (5) p. 939-946.

Chuvieco, E. Fundamentos de teledetección espacial. Madrid: Ed Rialp Tercera Edición, 1996.

Deepak, A., H. Fleming, and M. Chahine (eds.) (1986). *Advances in Remote Sensing Retrieval Methods*. A. Deepak Publishing, VA.

Dingman, S.L. 1994. Physical Hydrology. Upper Saddle River, NJ:Prentice Hall

Fusco, L. and Muirhead, K., 1987AVHRR Data Services in Europe- The Earthnet Approach, ESA Bulletin 49. p9-19.

Global Change Unit (cited as GCU). University of Valencia.www.uv.es/ucg Summer Course on Remote Sensing. Environmental Applications. Class notes, Course literature Compilation. Teruel July, 2005.

Gómez, M., Olioso, A., Sobrino, J. A., Jacob, F. (2005) Retrieval of evapotranspiration over the Alpilles/ReSeDa experimental site using airborne POLDER sensor and a thermal camera. *Remote Sensing of Environment, 399-408*

Hogan, D., Ouaidrari, H., and Shepard, M.(2000).Integrated algorithm design for global land surface temperature: An assessment for the new generation of environmental satellites. AGU 81 (48), Fall meeting.

Jiménez, J.C. Estimación de la temperatura y la emisividad de la superficie terrestre a partir de datos suministrados por sensores de alta resolución. University of Valencia. Doctoral Thesis, 2005.

Lee F. Johnson, Christine A. Hlacka, and David L. Peterson, "Multivariate Analysis of AVIRIS Data for Canopy Biochemical Estimation along the Oregon Transect ".*Remote Sense Of Environment*., 47, pp. 216-230. 1994.

Mc Clain, E. P., W.G. Pichel, and C.C. Walton (1985). Comparative performance of AVHRR- based multichannel sea surface temperatures . Journal of Geophysics Res., 90 11587-11601.

Mc Millin, L.M. and D.S. Crosby (1984). Theory and Validation of Multiple Window Sea surface temperature. Journal of Geophysics. Res., 89, 3655-3661.

Moreno, J., Calera, A., Caselles, V., Cisneros, J.M., Martinez-Lozano, J.A., Melia, J., Montero, F., Sobrino, J.A. (2001) *The measurement programme at Barrax.* Proceedings of the Final Results Workshop on DAISEX, ESTEC, Noordwijk, The Netherlands, 15-16 March 2001.

Millennium Ecosystem Assessment, 2005. *Ecosystems and Human Well-being: Synthesis*. Island Press, Washington, DC. Copyright © 2005 World Resources Institute

NOAA, 1999: NOAA KLM Users guide (on line): http://www2.ncdc.noaa.gov/docs/klm

Norman, J. Kustas W.P.and Humes, K.S. (1995). Two source approach for estimating soil and vegetation energy fluxes in observations of directional radiometric surface temperature. Agricultural and Forest Meteorology, 77, 263-293.

Pruitt, W.O. and Doorenbos J. 1977. Guidelines for predicting crop water requirements. FAO Irrigation and drainage Paper 24. FAO. Rome

Roerink, G.J., Su, Z., Menenti, M., 2000. S-SEBI A simple remote sensing algorithm to estimate the surface energy balance. Physics and Chemistry of the Earth. Part B: Hydrology, Oceans and Atmosphere 25 (2).p 147-157.

Shipert, P. (2004). Introduction to Hyperspectral image analysis. IDL Training Manual. Research Systems, Inc.

Sobrino, J.A., Gomez y M., Olioso, A. Estimación de la Evapotranspiraión en la zonas experimentales de Barrax y Alpilles a partir de imágenes del sensor DAIS. Revista de Teledetección 20 Dic. 2003.

Sobrino, J.A., Gomez, M., Olioso, A., Jacob F. Retrieval of Evapotranspiration over the Alpilles / ReSeDA experimental site using airborne POLDER sensor and thermal camera. Remote Sensing of the Environment 96 (2005) p 399-408.

SPARC Campaign web site. http://gpds.uv.es/sparc/

Thomas, G.E. and Stannes, K. (1999). *Radiative Transfer in the Atmosphere and Ocean*. Cambridge University Press.

Travis, L., Lacis, A., Multiple Scattering of Light by Particles. Radiative transfer and coherent Backscattering. Cambrige Press, 2006.

Vonder Haar, T., Kidder, S., Satellite Meteorology. Academic Press, 1995.